JOURNAL OF PETROLOGY | VOLUME 47 | NUMBER 12 | PAGES 2281–2302 | 2006 | doi:10.1093/petrology/egl044

Palaeozoic Intraplate Crustal Anatexis in the Mount Painter Province, South Australia: Timing, Thermal Budgets and the Role of Crustal Heat Production

SANDRA McLAREN[1]*, MIKE SANDIFORD[2], ROGER POWELL[2], NARELLE NEUMANN[3] AND JON WOODHEAD[2]

[1]RESEARCH SCHOOL OF EARTH SCIENCES, AUSTRALIAN NATIONAL UNIVERSITY, CANBERRA, AUSTRALIAN CAPITAL TERRITORY, 0200, AUSTRALIA

[2]SCHOOL OF EARTH SCIENCES, UNIVERSITY OF MELBOURNE, MELBOURNE, VICTORIA, 3010, AUSTRALIA

[3]GEOSCIENCE AUSTRALIA, GPO BOX 378, CANBERRA, AUSTRALIAN CAPITAL TERRITORY, 2601, AUSTRALIA

RECEIVED DECEMBER 16, 2005; ACCEPTED AUGUST 10, 2006; ADVANCE ACCESS PUBLICATION SEPTEMBER 8, 2006

The effect of radiogenic heat production within the crust on thermal processes such as crustal anatexis is generally disregarded as bulk geochemical models suggest that crustal heat generation rates are too low to effect significant heating. However, the Mount Painter Province in northern South Australia is characterized by a total crustal contribution to surface heat flow of more than twice the global average. The province is composed dominantly of Proterozoic granites and granite gneisses with an area average heat production of 16·1 $\mu W/m^3$; individual lithologies have heat production >60 $\mu W/m^3$. These Proterozoic rocks are intruded by the British Empire Granite, a younger intrusive whose origin has remained enigmatic. Isotope geochemistry suggests crustal sources for the melt and it has a crystallization age of $\sim$440–450 Ma, which places the setting >750 km inboard of the nearest active plate boundary zone at this time. Phase equilibria calculations suggest that temperatures of at least 720–750°C are required to produce the granite but the intensity of crustal thickening during Palaeozoic deformation ($\sim$12%) cannot account for these conditions. Here we describe a model for the generation of the British Empire Granite in which the primary thermal perturbation for mid-crustal anatexis was provided by the burial of the high heat-producing Mount Painter basement rocks beneath the known thickness of Neoproterozoic cover sediments. The high heat-producing rocks at Mount Painter imply that the natural range and variability of crustal heat production is much greater than previously believed, with important consequences for our understanding of temperature-dependent crustal processes including the exploitation of geothermal energy resources.

KEY WORDS: *geothermal energy; low-pressure anatexis; thermal conductivity; thermal regime*

INTRODUCTION

The thermal energy that drives crustal melting and other tectonic processes is ultimately related to heat loss from the Earth's interior; consequently our understanding of these processes is intimately connected with our understanding of the thermal structure of the Earth. Surface heat-flow data provide important constraints on the nature of lithospheric thermal regimes as they represent some function of the heat produced from radiogenic decay of heat-producing elements (U, Th and K) within the lithosphere, and the heat supplied to the base of the lithosphere by convection in the deeper mantle. Heat-flow, heat-production, seismic velocity models and other data suggest that the total contribution of crustal sources to the average surface heat flow is in the range 24–54 mW/m^2 (Table 1; Weaver & Tarney, 1984; Shaw *et al.*, 1986; Christensen & Mooney, 1995; Rudnick &

*Corresponding author. Present address: School of Earth Sciences, University of Melbourne, Melbourne, Victoria 3010, Australia. Telephone: +61 3 8344 7675. Fax: +61 3 8344 7761. E-mail: mclarens@unimelb.edu.au

Table 1: *Models of heat-producing element concentrations in bulk continental crust*

	U (ppm)	Th (ppm)	K_2O (%)	q_c (mW/m^2)
Geological models				
Weaver & Tarney (1984)	1·3	5·1	2·0	36
Shaw *et al.* (1986)	1·8	9·0	2·3	54
Taylor & McLennan (1981)	1·25	4·8	1·5	32
Taylor & McLennan (1985)	0·91	3·5	1·1	24
McLennan & Taylor (1996)	0·8–1·3	3·0–4·94	0·96–1·57	21–34
Seismic models				
Christensen & Mooney (1995)	(1·7)	(6·8)	2·1	45
Rudnick & Fountain (1995)	1·42	5·6	1·9	38
Wedepohl (1995)	1·7	8·5	2·4	51

Values in parentheses are from Rudnick *et al.* (1998), calculated assuming K/U = 104 and Th/U = 3·9. q_c, total crustal contribution to the surface heat flow, is calculated for each bulk composition, assuming a crustal thickness of 40 km.

Fountain, 1995). However, most attempts to understand crustal thermal processes have generally discounted the higher end of this range (e.g. Rudnick *et al.*, 1998), with the crustal contribution typically assumed to be around 20–40 mW/m^2 (e.g. McLennan & Taylor, 1996).

It has become increasingly clear, however, that the natural range and variability in continental heat flow is far greater than that suggested by simple arithmetic- or age-normalized averages of the heat-flow data and that these variations often represent significant differences in the relative contribution of crust and mantle sources. For example, Jaupart & Mareschal (1999) have shown that in many Archaean and Proterozoic provinces, heat-flow variations reflect large differences in bulk lithospheric composition and, in particular, crustal heat production. In these cases a 'global-means-approach' masks significant differences in thermal regime on the regional and terrane scale. Although the work of Jaupart & Mareschal (1999) represents a trend to challenging long-held beliefs about crustal thermal regimes, the natural variation in heat flow and heat production and the relative contributions of crust and mantle sources are still not well known. Our relatively limited knowledge of these parameters means that we have little appreciation of how the natural variation in the thermal parameter structure of the crust expresses itself in terms of thermally sensitive tectonic processes such as metamorphism and magmatism.

In a series of recent papers we have explored the extent to which anomalous heat production drives metamorphism in various settings associated with Australian Proterozoic crust (Sandiford & Hand, 1998; McLaren *et al.*, 1999; Sandiford *et al.*, 2002). This paper aims to extend that work to the realm of crustal anatexis by describing new data pertaining to shallow-level crustal anatexis in a zone of extremely anomalous heat production in the Mount Painter Province (MPP). The MPP is a small Proterozoic basement complex in northern South Australia (Fig. 1). Through a compilation of thermal property and other data, we show that the apparent high surface heat flow (126 mW/m^2; Sass *et al.*, 1976) is consistent with exceptional concentrations of heat-producing elements within the shallow crust (>60 μW/m^3 for some lithologies), with crustal contributions to the conductive surface heat flow plausibly greater than 80 mW/m^2. These values are extraordinary and must represent an extreme departure from global average crustal thermal regimes (Nyblade & Pollack, 1993). As the Mount Painter case is so extreme, it provides an exceptional natural laboratory to explore how anomalous heat production imposes on a variety of tectonic responses including crustal anatexis—the main focus of this paper.

REGIONAL SETTING

The Mount Painter Province forms the northernmost basement of the Adelaide Fold Belt in South Australia (Fig. 1). The province comprises the Mount Painter and Mount Babbage inliers. These basement inliers consist of high-grade metasediments of inferred Palaeoproterozoic age (Teale, 1993) that were subsequently intruded by Mesoproterozoic granites (Fig. 2). In turn, these rocks were overlain by a 12–15 km thick Neoproterozoic sedimentary sequence deposited during a series of rift-sag subsidence events from around 830 Ma (Preiss, 2000).

Broad subsidence controlled basin evolution from around 690 Ma until at least the early Cambrian at ~525 Ma. In the Southern Adelaide Fold Belt (Fig. 1) sedimentation appears to have been terminated by the onset of deformation and metamorphism during the Delamerian Orogeny. U–Pb zircon data from syn- and post-kinematic granites in the region constrain the Delamerian Orogeny to between 515 and 490 Ma (Jenkins & Sandiford, 1992; Foden *et al.*, 1999). Tectonism throughout the other parts of the Adelaide Fold Belt, including at Mount Painter, has also been ascribed to this event, largely on the basis of a similarity in structural style, and a pre-deformational depositional record that everywhere terminates at about the same time in the Early Cambrian (Jenkins & Sandiford, 1992).

In the Mount Painter Province the Palaeozoic deformation is typically thick-skinned, basement involved, and is characterized by the propagation of large-amplitude, basement-cored upright folds. Total shortening is estimated at only 12% (Paul *et al.*, 1999). Metamorphic

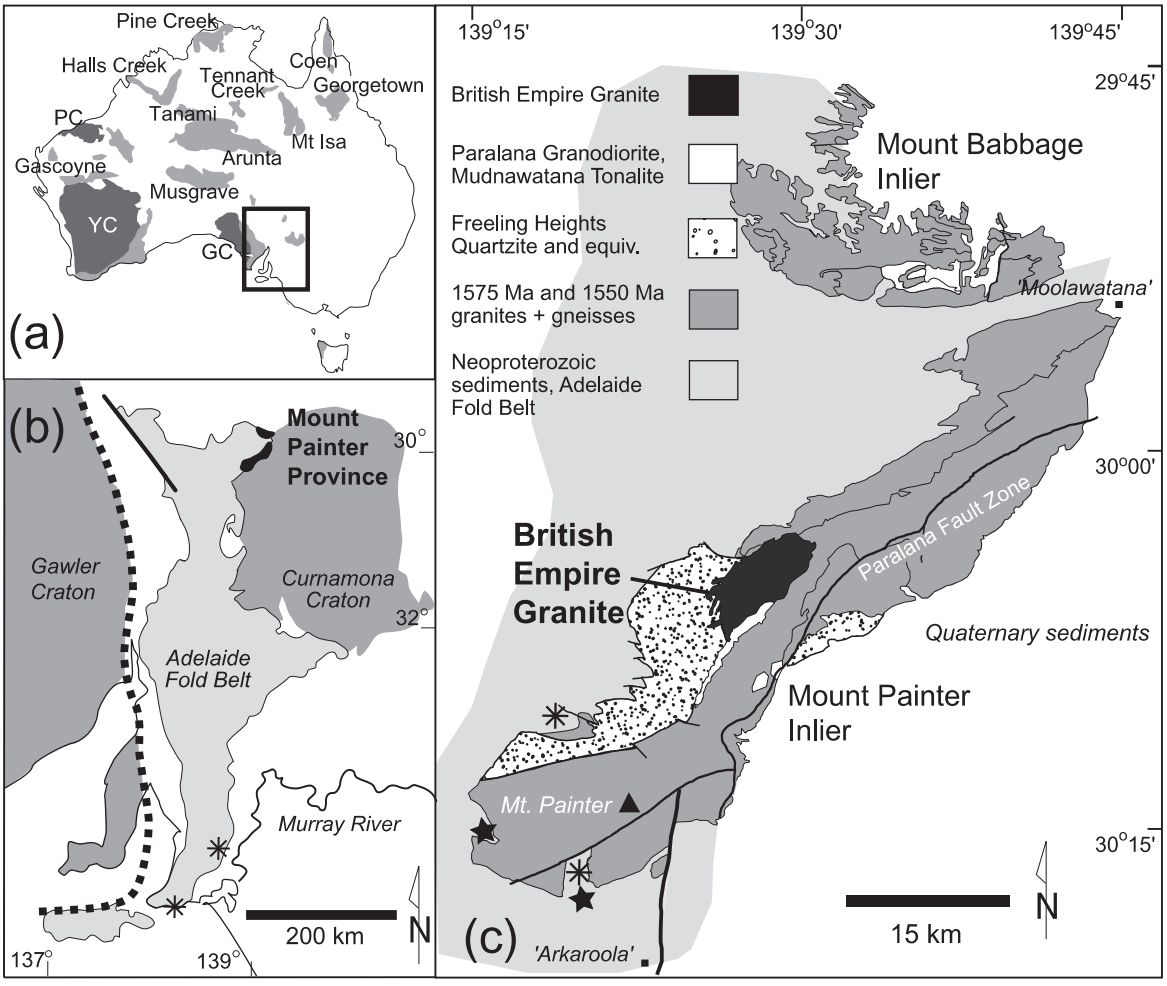

Fig. 1. (a) Location of the Mount Painter Province in northern South Australia. Location of other major Australian Proterozoic terranes is shown by light grey shading; that of Archaean cratons is shown by dark grey shading (YC, Yilgarn Craton; PC, Pilbara Craton; GC, Gawler Craton). Location of (b) is shown by box. (b) Structural framework of the Adelaide Fold Belt, showing the location of the Mount Painter Province (MPP) within the Adelaide Fold Belt. Also shown are the inferred extents of the Proterozoic Curnamona and Eastern Gawler cratons. Asterisks indicate locations where Delamerian Orogeny has been dated. (c) Sketch map of the southern and central Mount Painter inlier and the Mount Babbage inlier. Asterisks indicate locations of observed diopside-bearing assemblages; stars indicate locations of observed cordierite–anthophyllite assemblages.

assemblages in the cover and basement (including the growth of cordierite–anthophyllite- and diopside-bearing assemblages) indicate that the main fabric formed at low-pressure and relatively high-temperature conditions, of around 3–4 kbar and 500°C (Sandiford *et al.*, 1998). These data imply an average upper-crustal thermal gradient of 40°C/km. Given the relatively mild tectonic shortening and evidence that the cover sequence is ~12–15 km thick, the principal contribution to the pressure reflected in the metamorphic mineral assemblages appears to have been the accumulation of sediments during the Neoproterozoic. The Proterozoic granites and granite gneisses were subsequently intruded by a number of Palaeozoic igneous rocks, including the British Empire Granite, Paralana Granodiorite, Mudnawatana Tonalite and a number of small pegmatoidal bodies (Fig. 1).

PALAEOZOIC CRUSTAL ANATEXIS IN THE MOUNT PAINTER INLIER

General characteristics

Late-stage crustal anatexis is evident in the Mount Painter Inlier in the form of a number of small intrusive granites believed to be of Palaeozoic age. The largest of these is the British Empire Granite (BEG): a pegmatoidal garnet–muscovite granite, covering an area of around 23 km^2 in the central, structurally deepest part of the inlier (Figs 1 and 2). The BEG has long been thought to

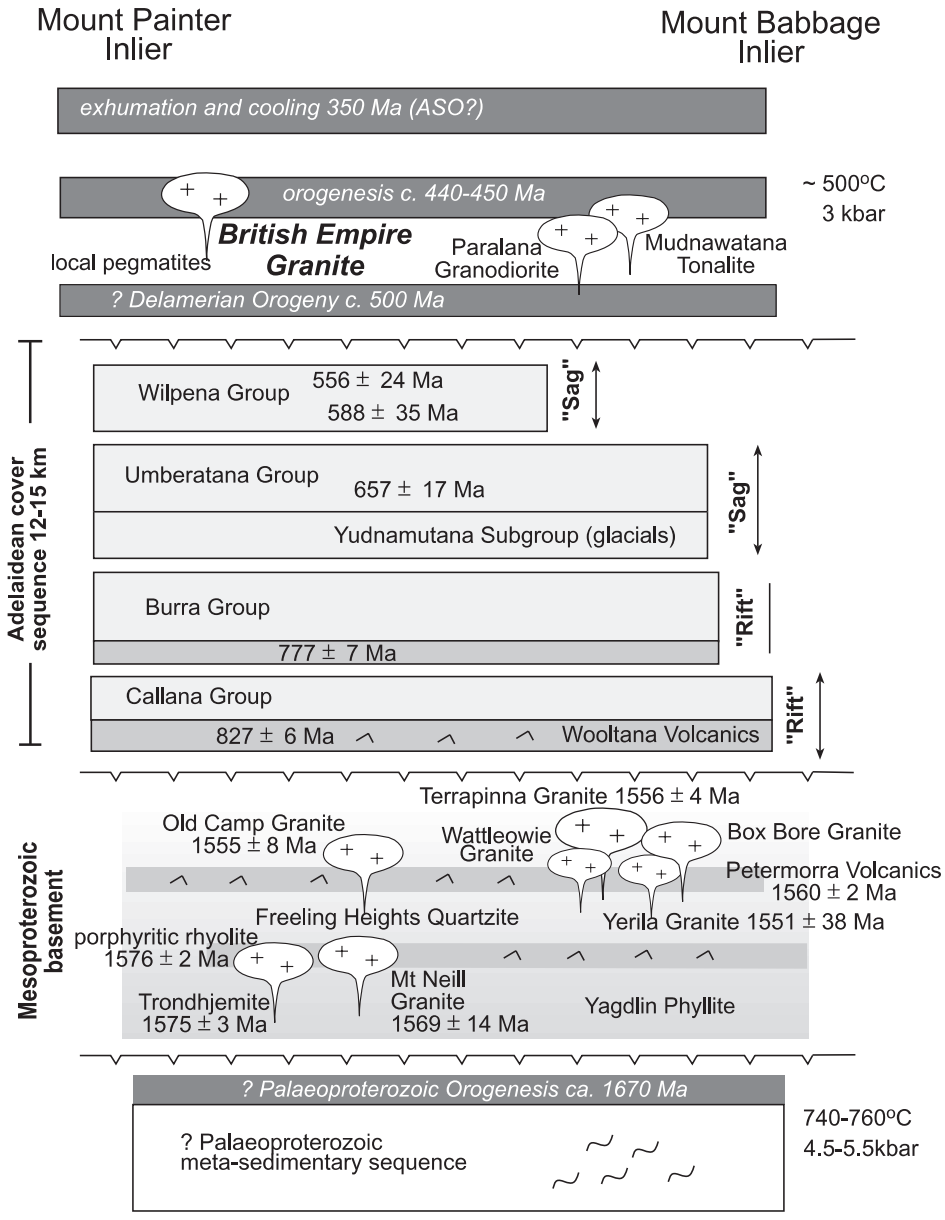

Fig. 2. Tectono-stratigraphic summary for the Mount Painter Province showing major magmatic, sedimentary and deformational events. Teale (1993) inferred the presence of Palaeoproterozoic rocks and metamorphism; however, there are no geochronological data to support this. Intrusive ages of Mesoproterozoic granites and volcanic rocks are those determined by U–Pb zircon geochronology; SHRIMP data are quoted where available. Terrapinna Granite age from Thornton (1980); MPI Trondhjemite age from Elburg *et al.* (2001); Yerila Granite age from Johnson (1980); Petermorra Volcanics age from Sheard *et al.* (1992); Old Camp Granite age from Fanning (1995); Mount Neil Granite and MPI rhyolite ages from G. Teale (1987, unpublished data). Age data for the Adelaidean cover sequence are summarized from Preiss (2000), and, with the exception of the age of the Wooltana Volcanics, are based largely on stratigraphic equivalence with units in the Southern Adelaide Fold Belt and central Flinders Ranges (where age data are largely SHRIMP U–Pb ages from zircons within cross-cutting dykes or interleaved tuffs). Exhumation at 450 Ma and 350 Ma has been dated in the southern MPI only (McLaren *et al.*, 2002) but almost certainly also affected the Mount Babbage Inlier (MBI). Toothed lines indicate major unconformities.

be a syn-tectonic Delamerian Orogeny intrusive, but its age has proved difficult to establish. Other Palaeozoic intrusives include the Mudnawatana Tonalite in the Mount Babbage Inlier and a dyke extending south from the BEG (Fig. 2). Recent work (Elburg *et al.*, 2003) has grouped this dyke with the BEG. However, we show below that the dyke is mineralogically, geochemically and isotopically distinct from the BEG and we follow Teale (1979) in distinguishing it as the 'Paralana Granodiorite'.

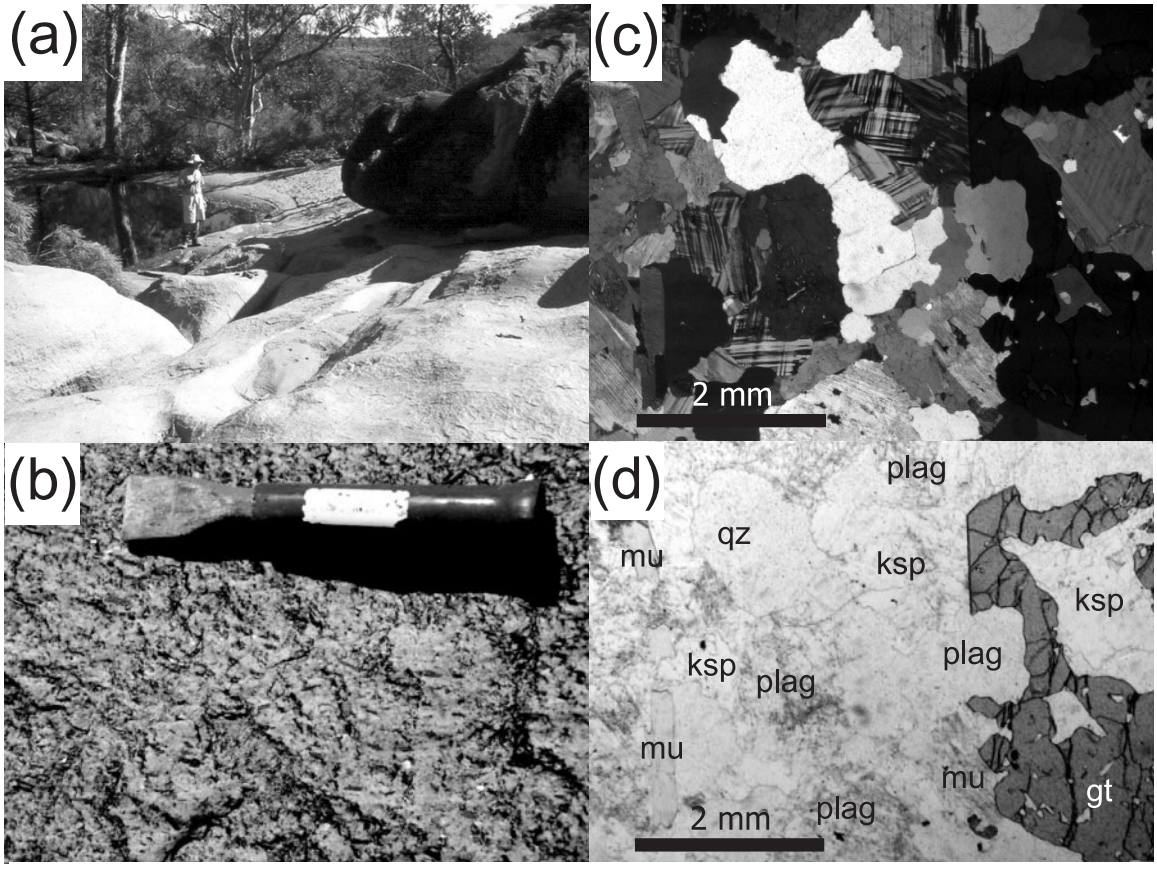

Fig. 3. (a) Extensive pavements of British Empire Granite in the region of sample 03-233, near the northeastern end of Hamilton Creek; sample locality (MGA94 coordinates, zone 54) 352025E/6674525N; (b) British Empire Granite in outcrop; chisel is 18 cm in length; (c) photomicrograph of coarse muscovite, K-feldspar–quartz texture; (d) photomicrograph of garnet phenocryst showing relationship of garnet growth to coarse igneous texture. gt, garnet; qz, quartz; plag, plagioclase; mu, muscovite.

On the outcrop scale the BEG is extremely heterogeneous, containing abundant biotite-rich schlieren up to 50 cm in size and, along its margins, xenoliths of the surrounding Proterozoic metasediments. Its grain size varies considerably, with abundant pegmatoidal segregations, particularly in structurally higher parts of the complex. The granite is surrounded by a narrow (<100 m wide) halo of migmatized metasediments, with a generally diffuse boundary between granite and migmatite. Structurally higher parts of the section/complex tend to be pegmatoidal. The granite contains coarse garnet, muscovite, K-feldspar, plagioclase, quartz and in some cases accessory tourmaline (Fig. 3). Muscovite and garnet within the granite are of similar grain size to the quartz and feldspar grains and are generally euhedral with good crystal terminations, suggesting that they are primary magmatic phases (e.g. Barbarin, 1996).

Geochemically, the BEG is a strongly peraluminous S-type granite and is characterized by ASI values [$Al_2O_3/(CaO + Na_2O + K_2O)$; Chappell & White, 1974] in the range 1·1–1·3. It is also characterized by relatively high silica contents, in the range 73·8–77·2 wt %, and relatively low total Mg, Ca and Ti concentrations (Table 2). As is common for peraluminous granites (Miller & Bradfish, 1980), the BEG is characterized by high initial $^{87}Sr/^{86}Sr$ ratios in the range 0·7540–0·7808.

In contrast to the BEG, the Paralana Granodiorite is a characteristically equigranular, medium- or coarse-grained granodiorite with plagioclase, quartz, biotite and minor K-feldspar and hornblende. Compositionally, its silica content ranges from 67·29 to 75·50 wt %, and it has elevated Al, Ca and Sr and high Na (6 wt % Na_2O). The Mudnawatana Tonalite has a small range in silica content from 72·2 to 73·0 wt % and has similar major and trace element concentrations to the Paralana Granodiorite. ASI values for both units range between 1 and 1·1, suggesting an I-type affinity (Table 2).

Neodymium isotope data suggest that the BEG is derived from largely crustal sources, with ε_{Nd} values in the range –12·5 to –14·4 at 440 Ma (Fig. 4). The

Table 2: Whole-rock geochemical analyses for key lithologies in the Mount Painter Province

Lithology:	British Empire Granite	British Empire Granite	British Empire Granite	Paralana Granodiorite	Paralana Granodiorite	Paralana Granodiorite	Mudnawatana Tonalite	Mudnawatana Tonalite	Freeling Heights Quartzite	Freeling Heights Quartzite
Sample no.:	A1086-MP1	A1015-HV-56	1077-389	99MP-1	99MP-3	A1086-PP2	97MP-58	99MP-11	A0186-NC3	A1086-NC4
Inlier:	Mt Painter	Mt Painter	Mt Painter	Mt Painter	Mt Painter	Mt Painter	Mt Babbage	Mt Babbage	Mt Painter	Mt Painter
Easting (AMG 54):	352350	354300	352230	352303	352214	350600	366246	366750	347300	347250
Northing (AMG 54):	6668700	6671100	6670820	6668299	6668513	6661200	6691798	6691700	6663500	6663500
%										
SiO_2	75·17	77·20	74·89	70·83	71·77	67·29	73·03	72·23	89·98	87·79
Al_2O_3	14·33	14·03	14·22	14·86	14·57	16·18	15·46	15·56	4·63	5·72
Fe_2O_3	0·52	0·47	1·07	1·92	1·78	2·77	1·18	1·49	2·78	2·34
MnO	0·01	0·01	0·04	0·03	0·03	0·02	0·03	0·03	0·01	0·01
MgO	0·18	0·12	0·25	0·62	0·58	1·12	0·48	0·60	0·21	0·44
CaO	0·48	0·60	0·54	1·81	1·72	1·84	2·19	2·35	0·01	0·02
Na_2O	3·50	4·27	3·77	3·35	3·35	4·44	5·12	5·31	0·06	0·16
K_2O	4·38	3·20	4·27	4·90	4·79	4·37	1·89	1·34	1·47	2·26
Ti_2O	0·05	0·04	0·06	0·33	0·31	0·55	0·14	0·19	0·17	0·22
P_2O_5	0·05	0·04	0·11	0·12	0·08	0·17	0·07	0·06	0·01	0·02
LOI	0·74	0·52	0·74	0·60	0·62	0·56	0·41	0·44	0·68	0·74
Total	99·41	100·49	99·97	99·39	99·61	99·30	99·98	99·61	100·02	99·71
ppm										
Rb	220·2	232·4	392·8	267·1	261·1	290·7	86·7	146·2	81·8	137·5
Ba	209	92·0	92	949	863	1202	300	186	448	443
Th	16·6	4·8	10·0	8·6	12·5	10·8	8·5	8·0	6·5	8·7
U	31·5	4·0	9·1	3·8	2·7	8·4	1·2	2·2	1·3	1·5
Nb	21·1	25·6	43·7	13·7	14·7	45·9	5·8	7·5	5·5	8·4
La	13	3·0	5	38	39	66	10	15	14	22
Ce	27	7·0	14	71	72	100	23	30	30	43
Pb	20·5	18·9	16·0	23·3	24·4	5·6	13·4	25·3	1	2
Sr	52·5	26·8	26·4	195·3	176·0	268·9	415·0	448·9	6·5	5·5
Nd	11	6·0	4	18	18	34	8	11	10	16
Zr	57·2	45·4	42·7	217·5	212·0	308·1	100·7	121·7	84	112
Y	38·5	23·3	19·3	4·2	8·1	43	7·2	18·8	10·7	13·6
Sc	3·3	5·1	1·8	2·2	2·9	5·8	1·8	2·8	2·1	2·9
Cr	0	4·0	283	14	3	16	0	5	11	12
V	5	5·2	8	18	17	31	11	16	25	17
Co	73	57·0	1	108	94	63	124	89	84	91
Ga	17·2	23·1	21·5	20·4	21·2	22·9	19·3	19·3	5·3	5·4
Cu	8	7·0	2	1	1	9	6	1	7	3
Zn	4	12·0	21	32	32	11	28	28	1	2
Ni	0	5·0	3	4	1	4	2	3	0	0

LOI, loss on ignition.

adjacent Paralana Granodiorite has less negative ε_{Nd} values around –7 to –10·5 at this time, with one sample recording a significantly more primitive value of –2·6. The Mudnawatana Tonalite has ε_{Nd} values within the range of the Paralana Granodiorite at 440 Ma. In terms of known representative protoliths, the isotopic variation of the BEG, Paralana Granodiorite and Mudnawatana Tonalite can be represented by mixing sources such as the Proterozoic metasediments and/or granites from the Mount Painter Inlier and the younger Neoproterozoic

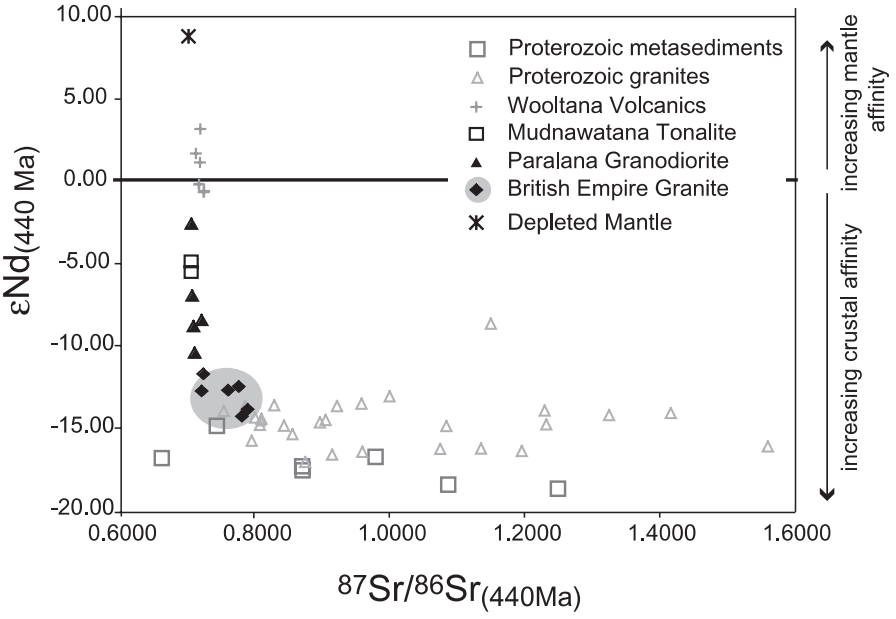

Fig. 4. Initial ε_{Nd} and $^{87}Sr/^{86}Sr$ isotopic ratios for major Proterozoic and Palaeozoic units of the Mount Painter Province, calculated at 440 Ma. Data are from Schaefer (1993), Neumann (2001) and Foden *et al.* (2002). Depleted mantle trace element and isotopic values are from Bell *et al.* (1982), Goldstein *et al.* (1984) and Sun & McDonough (1989).

Wooltana Volcanics from the lower parts of the cover sequences (Fig. 4). Further, the co-variation in Nd and Sr isotopic signatures between the S-type BEG and the I-type Paralana Granodiorite and Mudnawatana Tonalite suggests that these intrusives may be co-genetic, with the BEG containing a larger proportion of older, more evolved material than the granodioritic and tonalitic intrusives. Importantly, these values suggest that the BEG source must be largely crustal, with no, or only very limited additions from the mantle required to explain the observed Nd isotopic signatures. Moreover, the absence of evidence for heavy rare earth element (HREE) depletion (particularly Y) also points towards a shallow source in which plagioclase rather than garnet was stable (e.g. Singh & Johannes, 1996).

Geochronological constraints on Palaeozoic anatexis

The BEG has long been thought to be a syn-tectonic Delamerian intrusive, but reliable age data have previously proven difficult to obtain. Recently, however, Elburg *et al.* (2003) have reported a range of U–Pb isochron ages between 449 and 441 Ma for the granite, based on two-step leaching of monazite. Here, zircon and monazite grains were separated for sensitive high-resolution ion microprobe (SHRIMP) analysis, and magmatic garnets were subject to step leaching Pb isotopic analysis in an attempt to further constrain the crystallization age.

Zircon chronology

BEG zircons are highly variable in colour and morphology, ranging from deep yellow–brown largely anhedral to slightly subhedral grains, to colourless to slightly yellow-tinted euhedral grains with good crystal form (including doubly terminated crystals). U–Th–Pb isotopic ratios were determined for a selection of grains using the SHRIMP RG at the Australian National University. Owing to a high level of inheritance and extensive metamictization, almost all zircons analysed yielded highly discordant ages and hence do not constrain the crystallization age. Of the six concordant analyses, four are concordant at ~1550 Ma, raising the possibility that the granite was sourced at least in part from partial melting of the surrounding 1550 Ma granites and granite gneisses, and two were concordant in the range 460–440 Ma (see supplementary data, available at http://www.petrology.oxfordjournals.org).

Monazite chronology

BEG monazite grains are also variable in their colour and morphology. Two distinct populations have been recognized: (1) large (300–600 μm) yellow–brown grains; (2) small (100–200 μm) straw yellow grains with good crystal form. Back-scattered electron images reveal an unusual internal geometry, with many grains exhibiting a core of tetragonal crystal habit (similar to that which characterizes zircon) with anhedral overgrowths (Fig. 5). U–Th–Pb isotopic ratios were determined for a selection

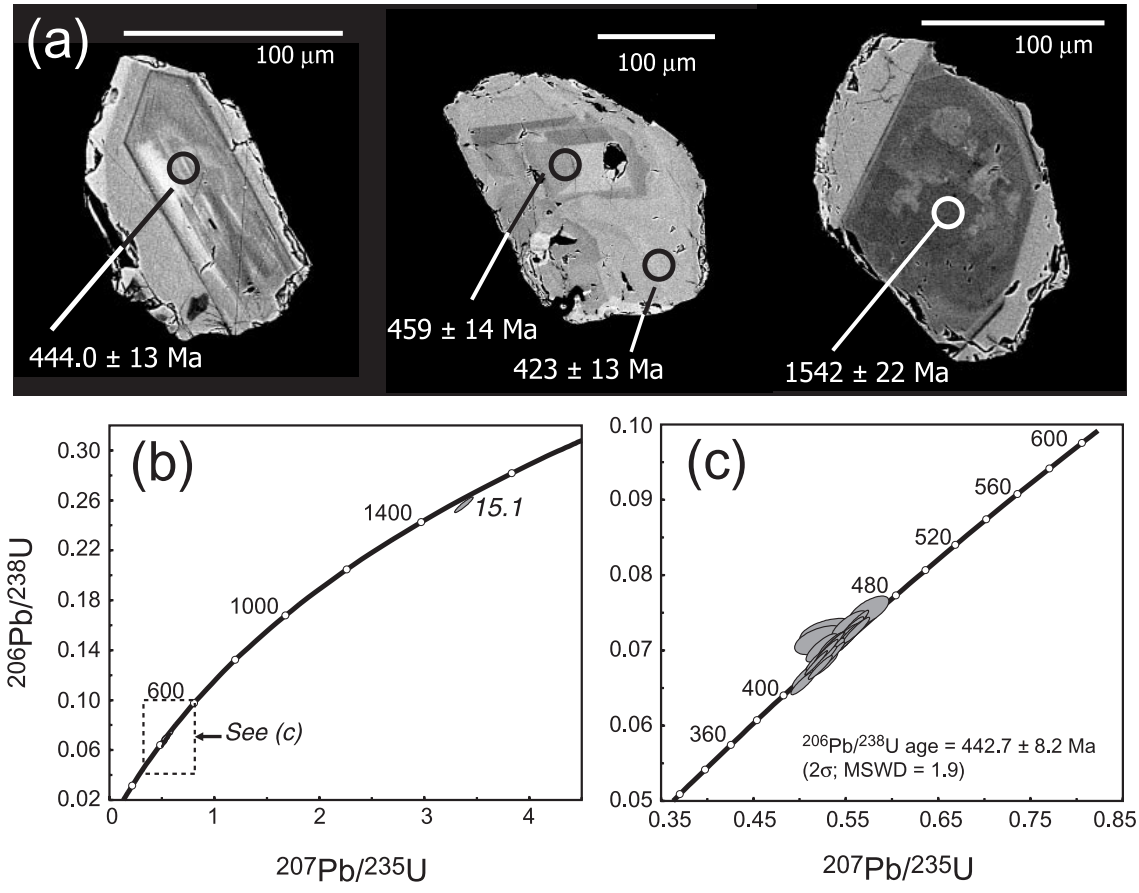

Fig. 5. (a) Representative back-scattered electron images of BEG monazites showing locations of SHRIMP analyses and ages; $^{206}Pb/^{238}U$ ages are given for Palaeozoic-aged grains, $^{207}Pb/^{206}Pb$ age is shown for Mesoproterozoic-aged grain. (b) U–Pb concordia diagram for all data indicating evidence for minor Mesoproterozoic inheritance; (b) enlarged section showing concordant Palaeozoic ages. Details of standard methods employed for SHRIMP analysis have been given by Compston *et al.* (1984) and Williams (1998).

of 24 monazite grains using the SHRIMP II at the Australian National University. The analytical procedure and data reduction routine have been described by Compston *et al.* (1984). The monazite data were all largely concordant (Fig. 5; supplementary data tables). One grain recorded a Mesoproterozoic age ($^{207}Pb/^{206}Pb = 1542 \pm 22$ Ma) consistent with inheritance from Mesoproterozoic sources. All other grains analysed recorded Palaeozoic ages. The weighted mean $^{206}Pb/^{238}U$ age is 442·7 ± 8·2 Ma (2σ error; MSWD = 1·9).

Garnet chronology

Two aliquots of magmatic garnet were subject to step leaching and Pb isotopic analysis, following the method of Frei & Kamber (1995). Three or four leachates, together with the residue, were analysed for each aliquot. These data reveal a wide range in $^{206}Pb/^{204}Pb$ and $^{207}Pb/^{204}Pb$ ratios (Table 3). As Frei & Kamber (1995) noted, garnet almost certainly contains microscopic and sub-microscopic Pb-bearing inclusions as well as trace

Table 3: Pb–Pb step-leaching data for garnet from the British Empire Granite

Analysis	$^{206}Pb/^{204}Pb$	$^{207}Pb/^{204}Pb$
Aliquot 1		
Leachate 1	249·254	29·227
Leachate 2	391·102	37·296
Leachate 3	2445·025	151·924
Leachate 4	108·623	21·448
Residue	129·702	22·690
Aliquot 2		
Leachate 1	530·636	45·099
Leachate 2	1093·297	76·417
Leachate 3	1928·587	123·514
Residue*	257·498	30·878

*The residue of aliquot 2 ran at low intensity and was thus excluded from the isochron calculation.

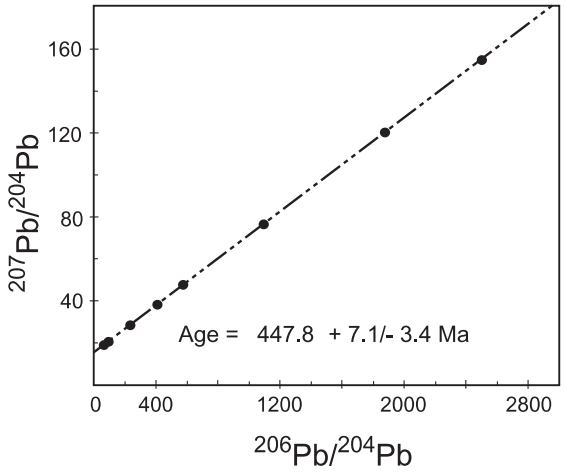

Fig. 6. $^{207}Pb/^{204}Pb$ vs $^{206}Pb/^{204}Pb$ mineral isochron from stepwise leaching of garnet from the BEG.

Pb within its own crystal structure, so this type of stepwise leaching can yield a mineral isochron to give the mineral age. For the BEG, the data from both aliquots yield a highly linear array (Fig. 6) with a $^{207}Pb/^{204}Pb$–$^{206}Pb/^{204}Pb$ isochron age of 447·8 Ma [+7·1 Ma, –3·4 Ma, using the robust statistical method of Powell *et al.* (2002)].

Elburg *et al.* (2003) reported a $^{207}Pb/^{235}U$ age of 442 ± 1·8 Ma and a $^{207}Pb/^{206}Pb$ age of 445 ± 2·5 Ma for monazite from the Paralana Granodiorite, obtained by two-step leaching. The similarity of the ages of the Paralana Granodiorite and the BEG suggest that the two intrusions were coeval.

Emplacement environment

Several lines of evidence point to elevated temperatures extending across the basement rocks of the MPP and into the lower parts of the cover sequence at the time of generation and emplacement of the BEG at ~440–450 Ma. Most importantly, the metamorphic mineral assemblages in the lower part of the cover sequence suggest average geothermal gradients in the upper 10 km of the crust of $\geq 40°C/km^1$ (see above). As noted previously by Mildren & Sandiford (1995) and Sandiford *et al.* (1998), the unusual pattern of isograds in the cover, paralleling the basement–cover unconformity, suggests that the unusual high heat-producing basement played a critical role in generating these thermal regimes.

Further quantitative constraints on the timing and duration of the 'high-geothermal gradient' metamorphic regime have been provided by McLaren *et al.* (2002), who reported K/Ar and $^{40}Ar/^{39}Ar$ data from the Mount Painter region. These data include a hornblende mineral separate from an amphibolite dyke adjacent to the Paralana Granodiorite that records an apparent K/Ar age of 423 ± 6 Ma and a well-defined $^{40}Ar/^{39}Ar$ plateau age of 432 ± 1 Ma. Hornblende samples from the southern Mount Painter Inlier (MPI) record K/Ar and $^{40}Ar/^{39}Ar$ ages in the range 500–445 Ma. These data suggest that rocks throughout the Mount Painter Province were at temperatures in excess of 500°C prior to 450 Ma and that the highest-grade rocks in the central MPI were at this temperature until around 430 Ma.

Finally, the Pb isotopic composition of K-feldspars from the 1575–1550 Ma granites in the MPP shows evidence of wholesale resetting in the Ordovician (Table 4). That such resetting has occurred is suggested by the fact that on a $^{207}Pb/^{204}Pb$–$^{206}Pb/^{204}Pb$ diagram (Fig. 7) the K-feldspars form a relatively well-defined linear array with a slope of 0·11037 ± 0·00061. This slope gives an 'age' of 1805 ± 10 Ma, older than the known crystallization ages of the Proterozoic granites (1575–1555 Ma; Fig. 2). Thus, it cannot be equated with the age of any physical process that affected the granites. To understand its significance we note that K-feldspar does not easily accommodate U, and thus its Pb isotopic signature changes very slowly with time unless it was opened to lead diffusion from its environment [for example, as a consequence of elevated temperature as suggested by Stacey & Kramers (1975)]. Let us consider that a K-feldspar starts with the Pb isotopic composition of the granite at the time of crystallization. After crystallization, the Pb isotopic composition of the K-feldspar barely changes, whereas the lead isotopic composition of the bulk granite evolves according to the bulk U/Pb (μ) value at the time of crystallization. If, at some later time, the granite experiences elevated temperatures (in excess of say, 500°C) and the K-feldspar is opened to Pb diffusion, the K-feldspar may preserve at least a partial record of the bulk Pb isotopic composition of the granite at that time. After 'closure' to Pb diffusion as a consequence of cooling, the K-feldspars would provide a palaeoisochron (Dickin, 1997, p. 129) from which the age of the K-feldspar Pb closure can be deduced, provided the age of the granite is independently known.

Considering that the trend of the K-feldspar data in Fig. 7a has significance in terms of a pseudo-isochron, Fig. 7b gives a K-feldspar Pb-closure age of 434 ± 33 Ma for a 1575–1555 Ma granite crystallization age. Figure 7a also shows the whole-rock Pb isotopic composition calculated for 450 Ma, showing that the data are consistent with this interpretation. Given that the K-feldspar Pb isotopic compositions are generally less radiogenic than those for the corresponding whole-rocks, isotopic equilibration may have been incomplete. The resulting K-feldspar isotopic composition will then be a mixture, with the Pb compositions falling along a mixing line essentially coincident with the trend of the K-feldspar and whole-rock data in Fig. 7a, thus little

Table 4: Pb isotopic data for selected Mesoproterozoic granites, Mount Painter Province

Sample	Description		U (ppm)	Th (ppm)	$^{206}Pb/^{204}Pb$	$^{207}Pb/^{204}Pb$	$^{208}Pb/^{204}Pb$
1077-308	Box Bore Granite	whole-rock	52·6	141·0	89·728	21·866	96·989
		K-feldspar			41·689	18·237	57·680
97-MP-56	Yerila Granite	whole-rock	138·6	454·9	152·216	26·824	172·366
		K-feldspar A			83·177	22·596	95·812
		K-feldspar B			82·832	22·536	95·318
97-MP-60	Yerila Granite	whole-rock	180·2	443·0	151·687	27·402	160·607
		K-feldspar A			91·306	23·658	96·193
		K-feldspar B			89·845	23·568	94·912
1077-363	Wattleowie Granite	whole-rock	9·2	37·4	23·302	16·091	42·666
		K-feldspar			21·197	15·985	40·675
1077-370	Wattleowie Granite	whole-rock	3·3	29·2	18·018	15·590	39·123
		K-feldspar			17·343	15·556	37·776
1077-381	Terrapinna Granite	whole-rock	13·0	58·9	21·461	15·920	43·029
		K-feldspar			18·911	15·717	39·367
97-MP-46	Terrapinna Granite	whole-rock	16·4	59·6	26·186	16·303	43·464
		K-feldspar			20·917	15·936	39·767

U and Th contents of K-feldspar leachates are generally very low (<1 ppm); A and B are two leachates from the same sample. In all cases the first leachate from each K-feldspar was not analysed, because of the probability of high common Pb content.

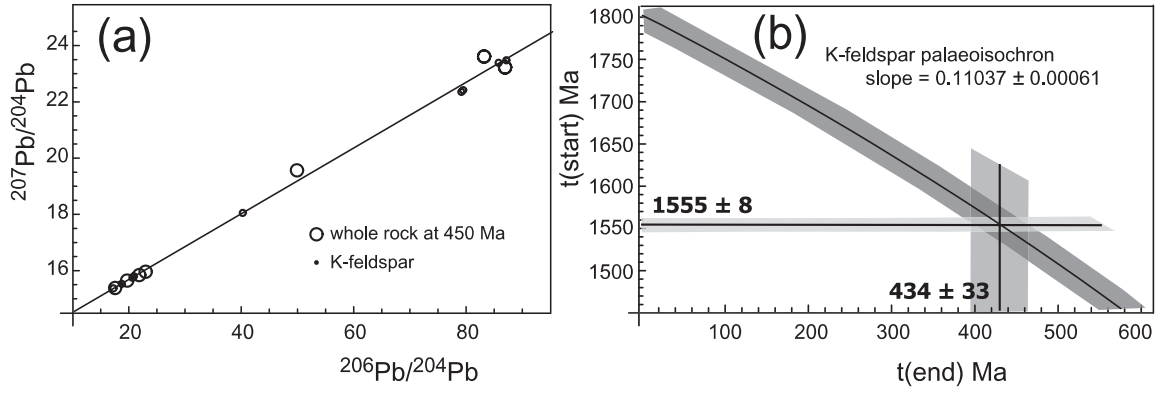

Fig. 7. (a) Pb–Pb isochron diagram for K-feldspar and whole-rock samples from various Mesoproterozoic granites in the Mount Painter Province. (b) Palaeoisochron, based on the slope of the isochron shown in (a). For the known age of the main group of Mesoproterozoic granites (1555 ± 8 Ma) a thermal event at 434 ± 33 Ma would be required to reset the K-feldspar Pb isotopic composition by Pb diffusion, assuming that the K-feldspars have remained closed to further diffusion since that time. *t(start)* represents the time at which the Pb isotopic composition was reset; *t(end)* represents the time at which the K-feldspar closed to Pb diffusion.

affecting the slope of the pseudo-isochron. Given that temperatures of at least 500°C are required for significant Pb diffusion in K-feldspar, these data provide support for the operation of such temperatures during the Ordovician.

Physical conditions of anatexis

Recent work by Holland & Powell (2001) and White *et al.* (2001) on partial melting phase equilibria in metamorphic systems allows the physical conditions of crustal anatexis to be addressed quantitatively in an analogous fashion to metamorphic geothermobarometry. The mineralogy and chemical composition of granitic systems, including the British Empire Granite, suggest that their origin can be considered in the Na_2O–CaO–K_2O–FeO–MgO–Al_2O_3–SiO_2–H_2O (NCKFMASH) system. To calculate phase relationships we use THERMOCALC (Powell *et al.*, 1998), the internally consistent dataset it uses (Holland & Powell, 1998), and

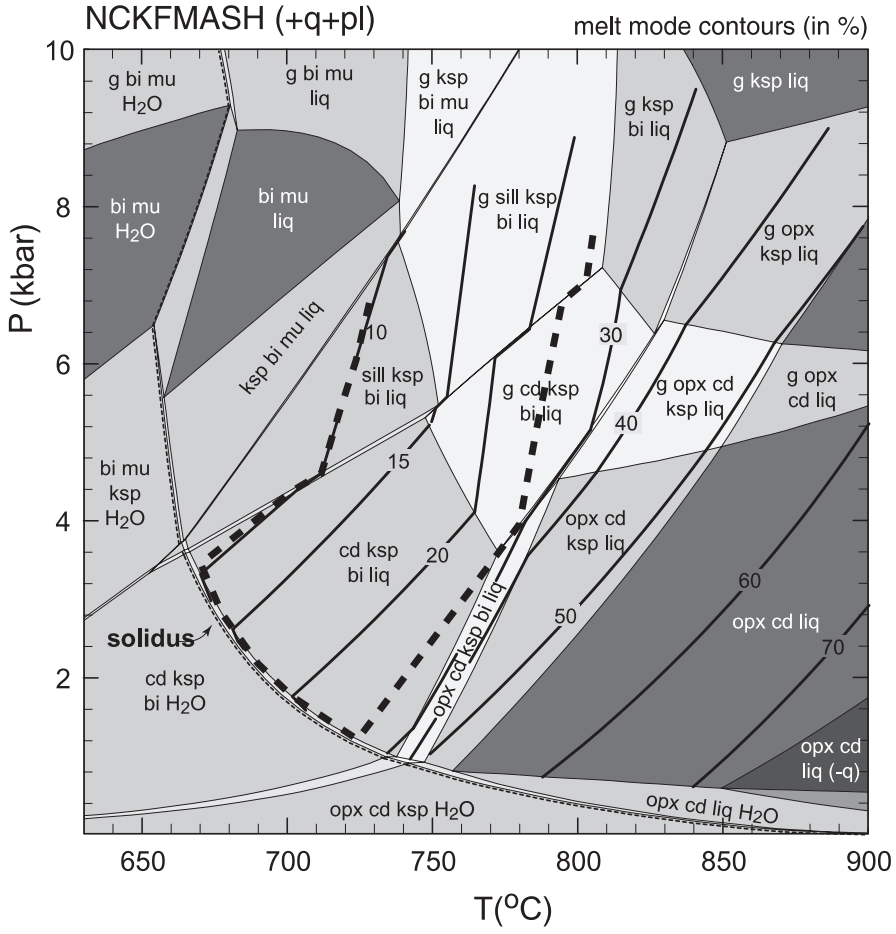

Fig. 8. NCKFMASH pseudosection calculated for a bulk composition of $H_2O = 6$, $SiO_2 = 75{\cdot}13$, $Al_2O_3 = 9{\cdot}62$, $CaO = 2{\cdot}69$, $MgO = 3{\cdot}67$, $FeO = 4{\cdot}27$, $K_2O = 2{\cdot}55$, $Na_2O = 2{\cdot}07$ (all values in mol %). Contours (bold lines) show the proportion of melt (%) in this rock composition. Lighter shading indicates an increase in the variance of the mineral assemblage. The dashed line outlines the minimum pressure–temperature conditions required for sufficient melting of the source, corresponding to around 10–25% melting, as discussed in the text (see Vigneresse *et al.*, 1996). It should be noted that for any given source bulk composition, the actual uncertainty on the position of the melt isopleths is around ±20°C. For the 20% melt isopleth the error is ±26°C. As discussed in the text, a more hydrous source composition will effect a bulk shift in the position of the melt isopleths to lower temperature.

the haplogranite melt activity–composition relationships of Holland & Powell (2001) and White *et al.* (2001).

In the absence of direct evidence of the source bulk composition, we show the nature of the phase relationships that will have controlled granite genesis using a calculated NCKFMASH pressure–temperature (*P–T*) pseudosection, contoured for the proportion of melt, for a mafic granite composition [using the mafic cordierite granite from the Bullenbalong Suite in the Lachlan Fold Belt, Australia (Chappell, 1996), with the following bulk composition: H_2O, 6 mol %; SiO_2, 75·13 mol %; Al_2O_3, 9·62 mol %; CaO, 2·69 mol %; MgO, 3·67 mol %; FeO, 4·27 mol %; K_2O, 2·55 mol %; Na_2O, 2·07 mol %] (Fig. 8). Such phase relationships are relatively constant for a wide range of metapelitic, semi-pelitic and granitic compositions, with the position of the melt proportion contours being essentially dependent on the proportion of micas in the starting mineralogy. As outlined above, as possible source rocks include the micaceous Freeling Heights Quartzite and the surrounding 1550 Ma granites and granite gneisses, we expect a relatively high proportion of available hydrous minerals, and potentially also free water, which may have migrated from the overlying Adelaidean basin along major crustal structures, including the basin-bounding Paralana Fault (Fig. 1). Thus, the phase relationships shown in Fig. 8 represent a conservative estimate of the temperature conditions appropriate to melting in the MPP.

The dashed line shown in Fig. 8 represents the range of melt proportions (from 10% to 25% melt) that might reasonably be expected to be able to escape from the

source. In the presence of non-coaxial strain, melt proportions possibly as low as 8% can escape from partially molten rocks. This is the so-called first percolation threshold (Vigneresse *et al.*, 1996). Perhaps more significant is the melt-escape threshold at around 20–25% melt production, associated with the loss of coherence in the source. From the point of view of generating the BEG, in the absence of other constraints, there is a trade-off between how extreme the thermal conditions are, and the volume of source that has to be processed to make the required volume of granitic magma, and also the volume of 'fertile' material that can actually produce magma. We note that, as Fig. 8 is constructed for a mafic granite composition, the position of the melt contours represent a conservative estimate of the thermal conditions required to generate appropriate amounts of melt. If the bulk source material prior to melting contained a higher proportion of hydrous minerals, or even minor proportions of free water had been added, then the position of the melt contours might shift to lower temperatures. For example, at 4 kbar the 20% melt isopleth corresponds to temperatures around 750°C, but this temperature may be lowered by up to 30°C for more hydrous source bulk compositions. Temperatures of around 700°C are considered to be a lower limit, as even in extreme cases where near solidus H_2O-fluxed melting is implicated, temperatures for anatexis are still above 680°C (White *et al.*, 2005). Thus, from a thermal point of view, we consider that temperatures in the range 720–750°C should be sufficient to produce the observed volume of British Empire Granite.

Regional correlation and origins of Palaeozoic anatexis in the MPP

The age data presented above allow for a reassessment of the regional correlations of crustal anatexis and deformation in the MPP, which have long been believed to have occurred during the Delamerian Orogeny (515–490 Ma, Foden *et al.*, 1999). The age data we have presented, together with other observations that point to elevated geothermal conditions at around 440 Ma, imply that tectonic activity in the MPP is more likely to be part of the earliest phase of a continent-scale, intraplate compressional regime associated with the initiation of the Alice Springs Orogeny at ~450–440 Ma (Mawby *et al.*, 1999; Scrimgeour & Raith, 2001) rather than the Delamerian Orogeny. Indeed, within the Mount Painter region, direct isotopic evidence for Delamerian activity is scant: Elburg *et al.* (2003) reported Delamerian-type ages of *c.* 500 Ma from a two-point K-feldspar, muscovite Rb–Sr isochron and a whole-rock and garnet Sm–Nd isochron from two deformed pegmatites. However, as it is difficult to evaluate the robustness of two-point mineral isochrons we cannot be certain of the significance of these data. Instead, we consider that at least some, if not all, of the deformation and metamorphism associated with the structuring of the inlier occurred around 440–450 Ma, coeval with the generation of the BEG.

THERMAL BUDGETS

One of the potential sources of heat for elevated thermal regimes in the Mount Painter crust is the anomalous heat production. In this section we assess the contribution of internal heat production in generating the conditions required for anatexis.

Background

The MPP forms part of a wide (>250 km) zone of anomalous heat flow centred on the Adelaide Fold Belt and Eastern Gawler Craton (Fig. 9). This zone was first identified by Sass & Lachenbruch (1979) and has been termed the South Australian Heat-flow Anomaly (SAHFA) by Neumann *et al.* (2000). Within the SAHFA surface heat-flow determinations from 11 distinct localities average 92 ± 10 mW/m^2. In terms of global averages this heat flow is anomalous. However, these values are not unusual in the context of other Australian Proterozoic terranes, where heat flow averages 83 mW/m^2 (Cull, 1982; McLaren *et al.*, 2003). As this high heat flow appears to be a regional phenomenon, it must result from either: recent tectonic, magmatic or hydrologic processes; anomalous mantle heat flow, or anomalous concentrations of heat-producing elements within the SAHFA lithosphere. Neumann *et al.* (2000) evaluated these possibilities and suggested that the anomalous heat flow is almost entirely of crustal origin. Indeed, the Neumann *et al.* (2000) analysis of seismic velocity and other data inferred a modern-day mantle heat flow of <30 mW/m^2, and possibly as low as 15 mW/m^2. These observations imply that crustal heat sources contribute at least 80 mW/m^2.

At present, there is only one heat-flow measurement, of 126 mW/m^2 (Sass *et al.*, 1976), from Parabarana Hill in the northern MPP (Fig. 9). Although this suggests that the MPP heat flow is slightly elevated compared with the SAHFA average, its full significance is not easy to evaluate, as the data are of low quality (Cull, 1982) and not well documented. Furthermore, the heat-flow site is in a relatively deeply dissected terrain within a few kilometres of the recently rejuvenated Mount Painter escarpment (Sandiford, 2003) and within 10 km of a small but active hot spring. Both of these phenomena are likely to have associated thermal transients that may have modified the measured heat flow.

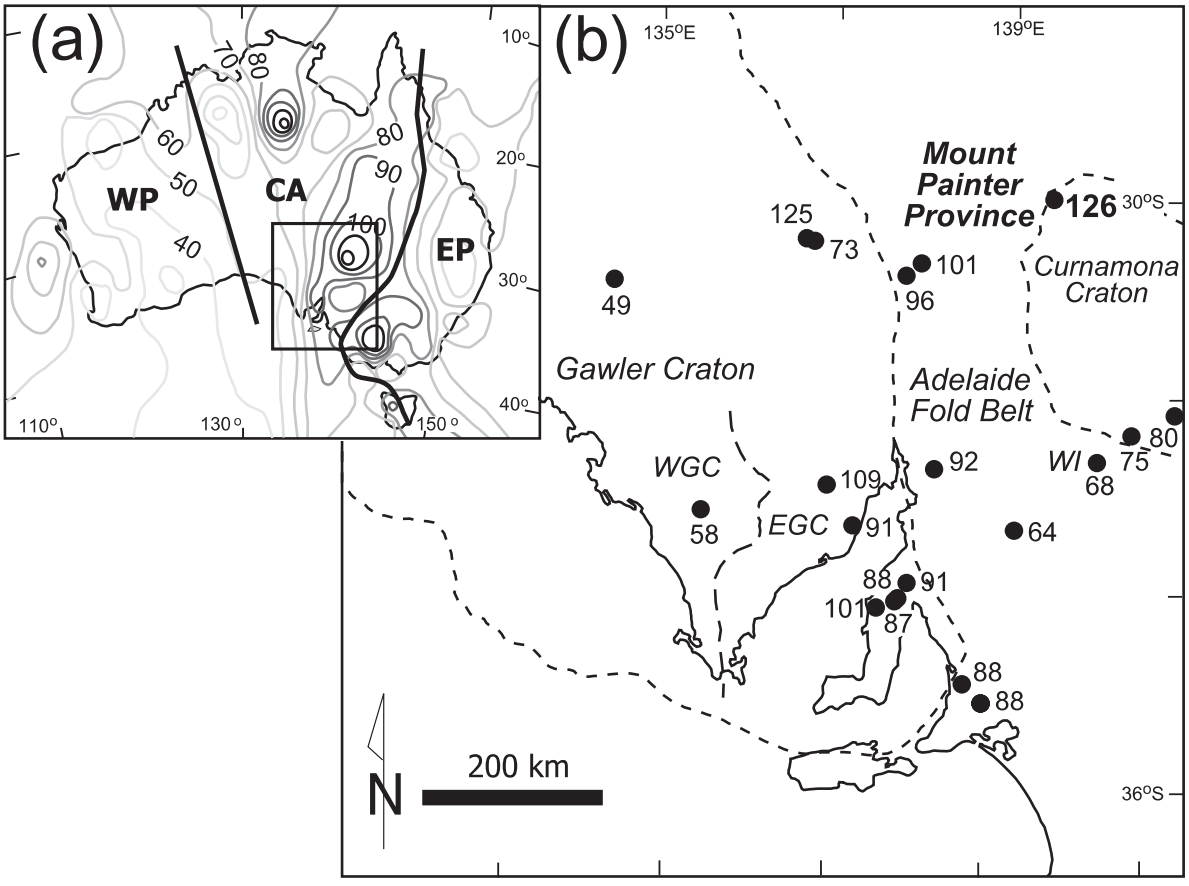

Fig. 9. (a) Australian heat-flow map. Approximate limits of the three Australian heat-flow provinces defined by Sass & Lachenbruch (1979) are shown. WP, Western Province; CA, Central Australian Heat-flow Province; EP, Eastern Province. Lighter grey contours represent lower heat-flow values; darker contours represent higher heat-flow values, as indicated. Values are heat flow in mW/m^2. (b) Heat-flow map for central South Australia showing the South Australian Heat-flow Anomaly (Neumann *et al.*, 2000). WGC, Western Gawler Craton; EGC, Eastern Gawler Craton; WI, Willyama Inliers.

Heat production

Heat-production values calculated from known concentrations of U, Th and K in surface lithologies (Table 5) support the notion that the MPP crust is exceptionally enriched in the heat-producing elements. These data suggest that almost all of the enrichment is contained within the Mesoproterozoic felsic igneous rocks of the Mount Painter and Mount Babbage inliers. When normalized by outcrop area (>400 km^2), heat production within these lithologies averages 16 $\mu W/m^3$.

Some individual granite stocks have heat production significantly above this average value (Table 5). These include the Hot Springs gneiss (41 $\mu W/m^3$) and the Box Bore granite (22 $\mu W/m^3$) in the Mount Painter inlier, and the Yerila granite in the Mount Babbage inlier (62 $\mu W/m^3$). When compared with average granite heat production of 2·5 $\mu W/m^3$, these values highlight the anomalous character of the MPP crust. The heat-producing element enrichment is restricted to the Proterozoic granites within the basement, with both the Mesoproterozoic and overlying Neoproterozoic sediments, and the younger granitoids, characterized by only average heat-production rates (Table 5).

The heat-producing element enrichment of the Mount Painter basement rocks is by far the most extreme of all the rock types within the SAHFA (Neumann *et al.*, 2000). It is also the highest amongst all the Australian Proterozoic felsic igneous rocks, which have an area normalized heat production of 4·6 $\mu W/m^3$ (McLaren *et al.*, 2003). Although these values are extreme this enrichment appears to be a primary igneous feature, rather than a product of secondary mobilization of U and/or Th in the near surface, as the Mount Painter rocks all have 'normal' Th/U values in the range of 2·7–5·8 (Table 5; Durrance, 1986). Interestingly, the most enriched granites also have the most 'normal' primary igneous Th/U values. For example, the Yerila Granite, with a calculated heat production of

Table 5: *Summary of geochemistry and heat-production data, Mount Painter Province*

Lithology	Area (km^2)	U (ppm)	Th (ppm)	K_2O (wt %)	Th/U	Q ($\mu W/m^3$)
Proterozoic granites						
Mount Neill Granite; Pepegoona Porphyry (60)	189	21	74	3·57	3·5	11·3
Terrapinna Granite (29)	99	10	58	5·24	5·8	7·2
Box Bore Granite (30)	40	44	131	6·37	3·0	21·6
Yerila Granite (28)	30	116	423	5·66	3·6	61·6
Hot Springs Gneiss (42)	22	75	288	4·17	3·8	41·0
Wattleowie Granite (27)	18	6	33	5·78	5·5	4·5
Petermorra Volcanics (7)	13	13	35	6·50	2·7	6·7
Average all Proterozoic granites, granite gneisses, felsic volcanics	411	29	110	4·62	3·8	16·1
Younger granites						
Paralana Granodiorite (26)	5	2·8	10·1	2·23	3·6	1·7
Mudnawatana Tonalite (4)	9	1·7	7·0	1·50	4·1	1·1
British Empire Granite (15)	23	11·5	8·9	4·2	0·8	4·1
Sediments						
Mesoproterozoic metasediments (9)		2·3	16·2	3·25		2·09
Adelaidean cover sequence (14)		3·4	12·7	5·28		2·33

Q is present-day heat production. The number in parentheses is the number of samples analysed. Mesoproterozoic metasediments include the Freeling Heights Quartzite and Yagdlin Phyllite. Granite data from Neumann *et al*. (2000); data for Mesoproterozoic sediments from Schaefer (1993) and Neumann (2001); data for Adelaidean cover sequence from O'Halloran (1992).

61·6 $\mu W/m^3$, has a Th/U value of 3·6, well within the accepted range for primary igneous rocks. The variation in observed Th/U values is not thought to be significant, largely because many important Th- and U-bearing phases (including zircon, monazite and xenotime) are known to have a much wider range of Th/U (Adams *et al.*, 1959), such that in whole-rock analysis the two elements do not necessarily show parallel variation. This is almost certainly the case for the MPP, as the majority of the Th and U is contained within accessory phases that appear to have crystallized prior to, or together with, the main rock-forming minerals.

Although it is possible that the available surface heat-flow measurement from the MPP is artificially elevated as a result of thermal transients associated with neotectonic activity and/or hydrological flow, available heat-production data suggest that the crustal contribution to the surface heat flow is extraordinary and suggest that the measured surface heat flow is likely to be around the actual heat-flow value. Conservatively, we suggest that crustal sources in the MPP contribute at least 80 mW/m^2 to the measured surface heat flow; the upper range of the SAHFA average (Neumann *et al.*, 2000). This value is exceptional when compared with global average models for the crustal contribution to surface heat flow (Table 1): more than three times the bulk crustal contribution suggested by McLennan & Taylor (1996) and Rudnick *et al.* (1998), and almost two times greater than the most radiogenic bulk crustal model of Shaw *et al.* (1986).

Distribution of crustal heat sources

Conductive thermal regimes in the crust are sensitive to both the abundance of heat- producing elements and their horizontal and vertical distribution. Here we outline some observations pertinent to the spatial variability of crustal heat production in the Mount Painter region consistent with known surface heat-flow constraints from the broader region encompassing the SAHFA. Treating the lithosphere as a one-dimensional (1-D) column, it is useful to describe the heat-production distribution using two parameters: h and q_c, without recourse to any assumptions about the specific form of the distribution (e.g. Sandiford & McLaren, 2002). The parameter q_c represents the crustal contribution to measured surface heat flow, and as outlined above, a conservative value for the MPP is 80 mW/m^2. The parameter h describes the effective vertical length scale over which this heat production is distributed. In general terms a strongly differentiated crust, in which much of the crustal heat production is contained within the upper crust, is characterized by low values of h, whereas undifferentiated crust is characterized by high values of h

(Sandiford & McLaren, 2002, 2006; McLaren *et al.*, 2005).

It is clear that the high values of surface heat production that characterize the MPP must be restricted to the uppermost crust, to be consistent with the average surface heat flow. Indeed, for $q_c = 80$ mW/m^2 a layer of average MPP granite (Table 5) only 5 km thick would be required to account for the entire crustal contribution. If 20 km of the middle crust contributes on average 1·2 μW/m^3 (e.g. Haenel *et al.*, 1988), then the thickness of MPP granite required is only 3·5 km. These observations suggest that the vertical distribution of heat sources within the modern MPP crust is highly differentiated and confined to the uppermost crustal column (i.e. low *h*).

Several lines of evidence suggest that the crustal heat production within the MPP basement is also strongly confined laterally. First, the metamorphic temperatures in the lower parts of the cover sequence seem to be significantly lower in an adjacent structural culmination, the Mount Burr diapir, around 30 km to the west (Fig. 1). Second, heat-flow measurements in the vicinity of the Roxby Downs Cu–U–Au–REE deposit (Fig. 1) show variations from 70 to 120 mW/m^2 on the 10–20 km scale (Houseman *et al.*, 1989), suggesting that the background heat flow within the northern SAHFA is around 70 mW/m^2. Third, spectral analysis of gravity and topography in the northern Flinders Ranges shows complex coherence at the 200–600 km scale, suggesting variable flexural properties, and hence thermal regimes, at length scales of <200 km (e.g. Simons *et al.*, 2000). Together these observations suggest that the Mount Painter thermal anomaly may be highly localized with a length scale of horizontal variability in heat production of only several tens of kilometres.

Modeling of thermal conditions prior to 450 Ma

Temperatures of around 700–750°C implied by the phase equilibria calculations clearly reflect anomalous thermal regimes. However, as outlined above, it seems unlikely that these thermal regimes result from any conventional process for anatexis. Here we assess the role that could be played by the high heat-producing Proterozoic granites and granite gneisses in generating the temperatures required for crustal melting.

Figure 10 shows the configuration and results from our 1-D thermal modeling. For our calculations we consider the crustal geometry of the Mount Painter Province including a maximum thickness Adelaidean sedimentary basin; that is, the configuration prior to deformation and metamorphism. The thermal property data used in our calculations are based on measured heat production and thermal conductivity values from individual lithologies

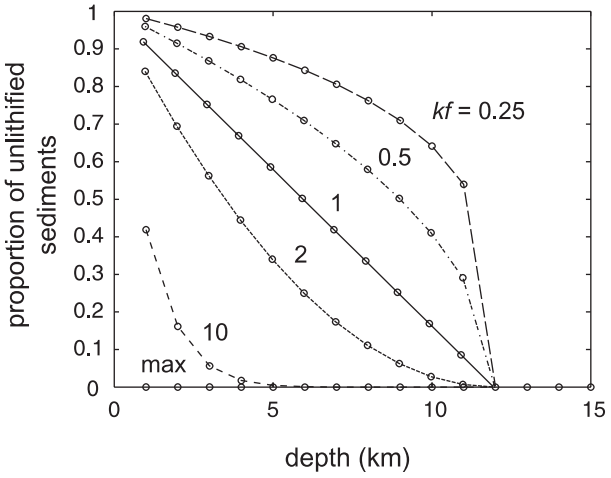

Fig. 10. Possible variations in thermal conductivity with depth for the Adelaidean basin sediments. The parameter *kf* indicates the relative ratio of unlithified thermal conductivity to lithified thermal conductivity over the 12 km thickness of the basin. As discussed in the text, values of $kf \geq 1$ are considered most likely. Here, all thermal conductivity functions vary over 12 km, the maximum depth of the sedimentary basin.

(Tables 5 and 6). We take conservative estimates of heat production and thickness of the granites, allowing a two-layer geometry for the high heat-producing basement: the uppermost granite layer is 4 km thick and has a heat-production value of 10 μW/m^3 and the deeper layer is 5 km thick with average heat production of 5 μW/m^3. We note that very similar model results are obtained for a thinner, but higher average heat-production granite layer. The 20 km of the lower crust has a heat production of 1 μW/m^3 such that the total basement heat flow is 85 mW/m^2. Heat production within the Neoproterozoic cover sediments (Table 5) contributes a further 30 mW/m^2 to the total pre-orogenic surface heat flow. As the basin was subsiding and sediments were accumulating from 800 Ma until at least 500 Ma, the mantle heat flow is likely to have been relatively low by the end of this interval, and in the following discussion we assume a value of ~10 mW/m^2. These values of heat production and mantle heat flow give a 1-D surface heat flow at 450 Ma of 125 mW/m^2, and a heat flow at the top of the high heat-producing basement of 100 mW/m^2, which is at the lower end of the range based on the observed heat-production and heat-flow data.

The thermal conductivity of each of the major sequences of the Neoproterozoic cover sequence (Table 6) has been measured using a divided bar apparatus, and these data provide an important constraint for our calculations. Table 6 also shows averages of unlithified sediments as determined by Periera *et al.* (1986). The thermal conductivity of the

Table 6: Average thermal conductivity of the Adelaidean basin, Mount Painter Province

Group or Unit	Lithology	Estimated thickness (km)	Estimated thickness (%)	Conductivity (W/m per K) lithified	Conductivity (W/m per K) unlithified	Heat production ($\mu W/m^3$)
Callana Group	SAND	0·8	6·3	4·3	2·0	1·89
	CARB	0·8	6·3	3·7	1·8	3·47
	S/S	0·8	6·3	1·9	1·2	2·39
Burra Group	SAND	0·3	2·2	4·3	2·0	1·89
	CARB	1·2	9·8	3·7	1·8	3·47
	S/S	1·8	15·3	1·9	1·2	2·39
Lower Umberatana Group	S/S	1·4	11·9	1·9	1·2	2·39
Middle–Upper Umberatana Group	CARB	0·3	2·4	3·7	1·8	3·47
	S/S	0·4	2·9	1·9	1·2	2·39
Brachina Group	S/S	0·0	0·0	1·9	1·2	2·39
Bunyeroo Formation	S/S	3·3	27·3	1·9	1·2	2·39
Wonoka Formation	S/S	0·0	0·0	1·9	1·2	2·39
Upper Wilpena Group	SAND	0·6	4·7	4·3	2·0	1·89
	S/S	0·6	4·7	1·9	1·2	2·39
Total/Average		12·0				2·50

A standard divided-bar apparatus was used to measure the contemporary thermal conductivity of each of the major sedimentary units within the cover sequence. The values listed here are an average of all analyses for each lithotype: SAND = sandstones or quartzites (8); CARB = carbonates (8); S/S = siltstones or shales (6). Pre-deformational thicknesses are from restored structural cross-sections of Paul *et al*. (1999).

equivalent unlithified sediments is significantly lower than that of the lithified sediments, as a result of the combined effects of porosity, lower temperature and water saturation (e.g. Dovenyi & Horvath, 1988). As lithification of the sequence must have been progressive during burial, we assume that the data for lithified and unlithified sediments provide upper and lower bounds, respectively, on the actual thermal conductivity of the Neoproterozoic cover sequence. We investigate the effect of a range of thermal conductivity models for the Neoproterozoic cover sequence in detail below. The thermal conductivity of the basement granites and typical lower crustal rock types were not measured and we assume an average value of 3·2 W/m per K for these units (e.g. Haenel *et al.*, 1988).

The thermal structure through the MPP crust is sensitive to the thermal conductivity structure of the sedimentary basin sequence (e.g. Fig. 10). We have explored different parameterized models for the depth dependence of the basin thermal conductivity in a range between the upper and lower limits provided by the lithified and unlithified thermal conductivity data (Table 6; Fig. 11). As it is likely that the thermal conductivity of the sediments increases with depth, as a result of progressively lithification, we employ a simple parameterization based on a parameter we term kf. For $kf = 1$, thermal conductivity increases linearly with depth from the average unlithified value at the top of the sedimentary pile to the average lithified value at the base of the sedimentary pile (Fig. 11, Table 6). A value of $kf > 1$ indicates a higher proportion of lithified sediment and $kf < 1$ indicates a higher proportion of unlithified sediment. Intuitively, $kf \geq 1$ would seem most likely, with low values of kf (indicating low thermal conductivity throughout the 12 km sedimentary sequence) considered less likely. Values of $kf > \sim 5$ correspond to an almost completely lithified sequence with a limiting temperature at the base of the sedimentary pile ($T_{c\text{-}b}$) of 525°C for our heat-production model. Values of $kf \ll 0{\cdot}25$ correspond to an almost completely unlithified sequence with a limiting $T_{c\text{-}b}$ of ~850°C.

A 1-D analysis of the steady-state thermal regime appropriate to this configuration allows us to make predictions about the temperature structure of the crust in the MPP (Fig. 10). Independently of the details of the thermal conductivity structure of the cover, the high heat-producing basement sequence, and low conductivity sedimentary package means that high geothermal gradients of ~45°C/km propagate throughout the sedimentary pile (see also Sandiford *et al.*, 1998). The relatively low heat flow from the lower crust and mantle results in low thermal gradients beneath the high heat-producing granites (~10–15°C/km), giving a strongly 'kinked' geotherm (Fig. 10).

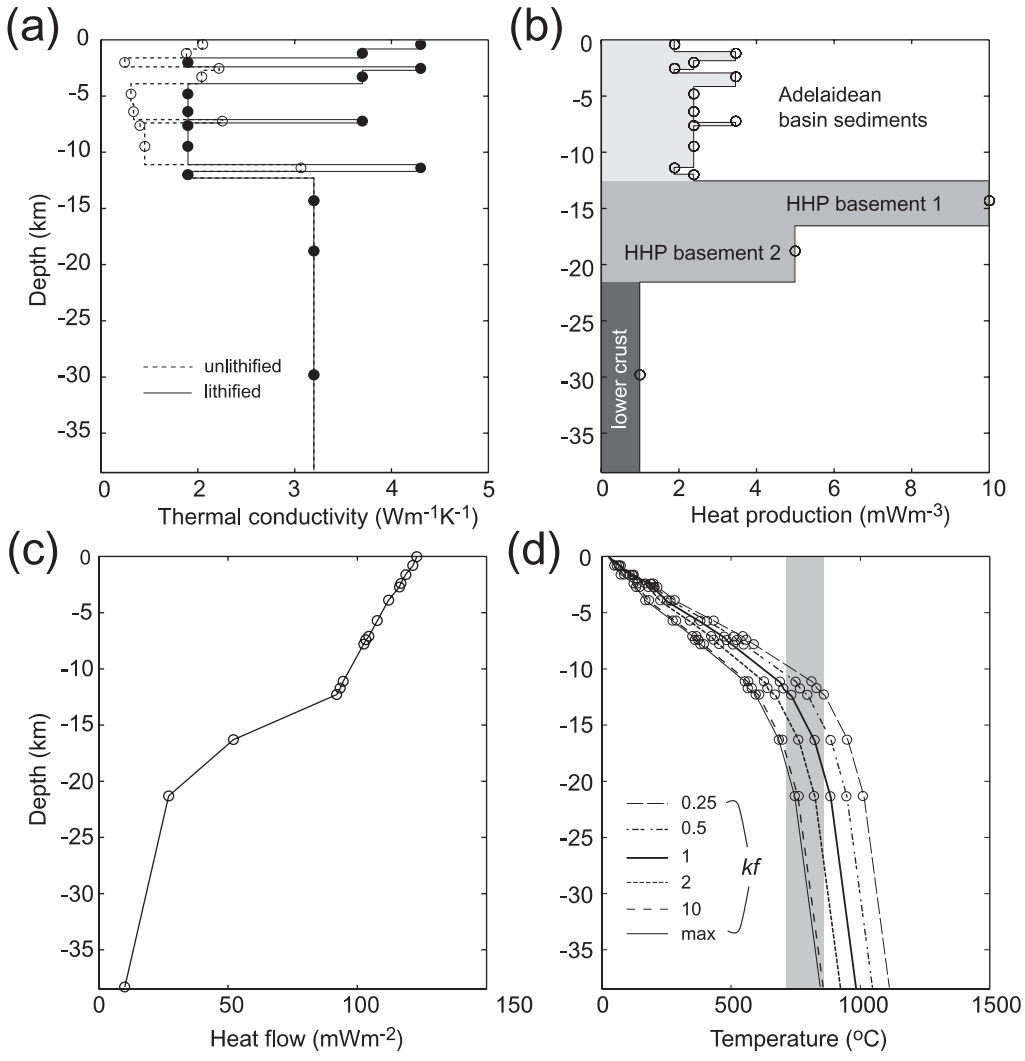

Fig. 11. (a) Thermal conductivity data used in modeling routines. Only end-member lithified and unlithified thermal conductivity models are shown for the Adelaidean basin sediments. (b) Variation in heat-production data with depth used in modeling (see also Table 5). The 1-D model for the configuration of the Mount Painter Province crust prior to deformation and metamorphism is also shown. HHP basement, high heat-producing basement. (c) Calculated heat flow with depth. Mantle heat flow = 10 mW/m^2, total surface heat flow = 125 mW/m^2 and the heat flow at the top of the heat-producing layer = 100 mW/m^2. (d) Calculated crustal geotherms for a range of thermal conductivity models corresponding to *kf* values 0·25, 0·5, 1, 2 and 10. The required melting temperature of *c.* 725°C is indicated.

For values of *kf* in the range 0·25–10, $T_{c\text{-}b}$ ranges from ~850 to 525°C, with the highest temperatures corresponding to the lower average thermal conductivity models (Fig. 10) where *kf* <1. For this range, temperatures required for generating the BEG (i.e. >720°C) are achieved at depths between 18 and 10 km. Temperatures at the base of the crust (at depth 40 km) range from around 825°C to almost 1100°C (Fig. 10).

The upper end of this range of modeled lower crustal temperatures, which corresponds to the models with the highest mid-crustal temperatures, is clearly extreme. Such high temperatures exceed the likely threshold for rheological stability, and would be expected to result in wholesale melting of the lower crust. However, if we consider two-dimensional (2-D) models where the high heat-producing layer is laterally confined, the geothermal gradients below the level of the heat-producing layer are suppressed because of the lateral flow of heat away from the high heat-producing rocks. To demonstrate this we use an analytical approximation to the high heat-producing basement in the 1-D models in which basement heat production decays exponentially from some maximum over characteristic length scales in both the vertical and horizontal directions. Thus, for all models heat production decays to e^{-1} of its maximum value over a vertical length scale of 3·3 km. In the

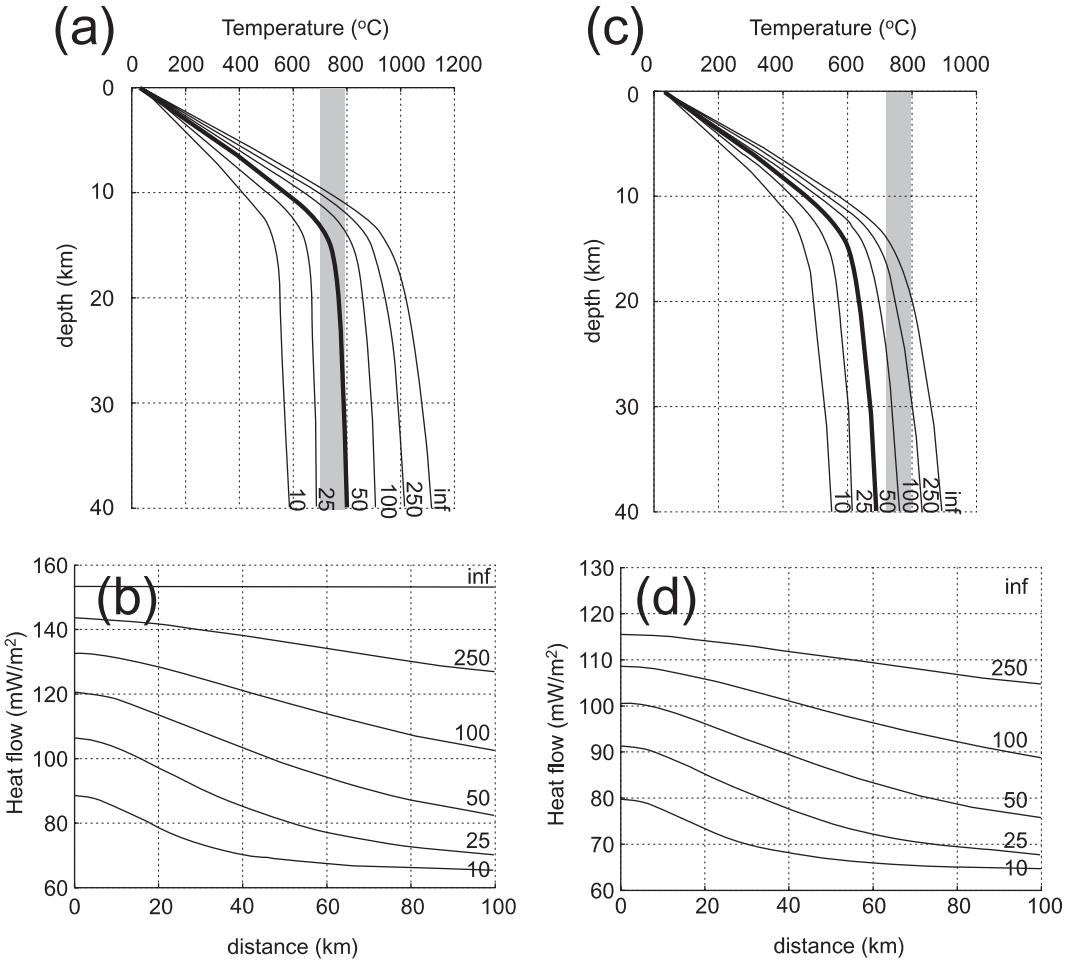

Fig. 12. Results of 2-D thermal modeling in which the high heat-producing granite layers are confined laterally. The shaded regions in (a) and (c) represent the thermal conditions required for melting. In these models the heat production decays to e^{-1} of its maximum value over a horizontal distance, h_x, of 10, 25, 50, 100, 250 km or ∞ (equivalent to the 1-D model). (a) Geothermal gradients and (b) calculated surface heat flow as a function of distance for a model with maximum basement heat production of 21 mW/m^3. Temperatures in the middle crust exceed that required for melting for all models with $h_x > \sim 30$. It should be noted that for $h_x = 50$ km, the total heat flow from the basement is 120 mW/m^2, which corresponds well to the observed modern-day heat-flow value. For comparison, (c) geothermal gradients and (d) calculated surface heat flow as a function of distance for a low heat-production model with maximum basement heat production of 14 mW/m^3. Temperatures in the middle crust do not approach that required for melting.

horizontal dimension, basement heat production decays to e^{-1} of its maximum value over a variable horizontal distance, h_x. We assume a heat-production maximum at 14 km depth, consistent with burial of the enriched basement beneath the sedimentary cover. The heat production of the sedimentary basin units is an average of the measured values (Table 5), giving the same contribution to the surface heat flow and heat production in the lower crust as in the 1-D models.

For 2-D models with a maximum basement heat production of 21 μW/m^3 and a horizontal length scale of around 50 km (see previous discussion) temperatures at a depth of 15 km are ~720°C. At the same time, lower crustal temperatures are limited to around 800°C (Fig. 12). Such a laterally confined heat-production distribution is the only way to achieve high mid-crustal temperatures without extensive lower crustal melting. We expect that the MPP lower crust was rather refractory following extraction of the voluminous Mesoproterozoic granites, and so lower crustal temperatures of ~800°C are unlikely to cause wholesale melt extraction from the lower crust, nor significant rheological instability. However, these temperatures are still elevated compared with normal geothermal gradient conditions and may have caused some localized lower crustal melting. This scenario is consistent with the observed small-volume Paralana Granodiorite in the Mount Painter Inlier and Mudnawatana Tonalite in

the Mount Babbage Inlier, and we suggest that these intrusives represent products of minor lower crustal melting.

Temperatures of around 550–600°C at 12 km depth at the base of the sedimentary basin predicted from both the 1-D and 2-D modeling agree well with the observed metamorphic conditions along the basement–cover interface (Fig. 1). However, temperatures at this depth, in all but the lowest conductivity models, do not reach the values of 720–750°C required for melting, as implied by the phase equilibria calculations. Temperatures of 720–750°C are reached at depths of between 9 and 17 km for 1-D models, depending on thermal conductivity variation (Fig. 10). For $kf \geq 1$, temperatures exceed 720°C at depths around 16 km (Fig. 10).

Attainment of the thermal conditions required for the generation of the BEG melt at around 15–16 km depth, at the level of the Proterozoic granites and metasedimentary rocks, is consistent with the composition of the inferred source rocks based on the available geochemical and isotopic data. If the melt was generated at these depths it would need to move less than 2 or 3 km up the crustal column to its present site. This scenario suggests that the migmatitic sediments present along the granite margins are a consequence of the advection of heat from depth and that the modern BEG represents a 'pooling' site for melt generated at deeper crustal levels. Melting at around mid-crustal levels is also consistent with the observed REE signature that points towards a shallow source containing plagioclase rather than garnet.

The calculations presented here show that for a plausible range of thermal properties based on measured values, the burial of the radiogenic basement granites beneath the Adelaidean cover is able to account for the thermal conditions required for the generation of the BEG. Low mantle heat flow and the lateral flow of heat from a horizontally confined high heat-producing basement rocks act to suppress the deeper crustal geotherm, limiting significant lower crustal melting. Limited crustal thickening during orogeny, and the advection of heat from some limited lower crustal melting may have also provided additional heat to the middle crust. The Mount Painter example is extreme, but suggests that the burial of rocks enriched in the heat-producing elements is capable of driving not only high geothermal gradient orogeny (McLaren *et al.*, 1999) but also localized crustal anatexis.

DISCUSSION

The heat source for Palaeozoic anatexis in the Mount Painter Province has long remained enigmatic. We have constrained the temperatures required for the generation of the British Empire Granite using phase equilibria calculations and described a model in which the primary thermal perturbation for melting arises as a consequence of the burial of Proterozoic high heat-producing granites beneath a thick sedimentary cover. Low mantle heat flow consistent with basin fill accumulation, together with lateral heat flow away from the basement heat-production anomaly, act to suppress lower crustal geothermal gradients and limit lower crustal melting. This model appears to account for the timing of magmatism and the geochemistry of the magmas, as well as the observed intrusive relationships. The burial of the extraordinary high heat-producing basement rocks significantly weakened the MPP crust and the Palaeozoic deformation, metamorphism and magmatism appear to be a direct response to this thermo-mechanical instability. Indeed, deformation and magmatism in response to external tectonic forcing associated with the initiation of the Alice Springs orogeny probably acted as 'safety valves' in exhuming the high heat-producing rocks and terminating orogeny as crustal temperatures became extreme. Exhumation of the high heat-producing rocks to their present-day position in the uppermost crust effected a significant increase in thermal and mechanical stability, allowing the extreme heat-production enrichment to be preserved.

Although the Mount Painter case is extreme by global standards its preservation suggests that the amplitude of heat-production variation within the crust, as well as the natural horizontal length scale of that heat production, is highly variable. Moreover, the Mount Painter example suggests that the amplitude and length scale of heat-production variations in the crust are related such that rocks highly enriched in the heat-producing elements can be thermally and mechanically stable provided their horizontal length scale is short compared with the typical thickness of the crust. The Mount Painter example also illustrates the importance of vertical differentiation of the heat-producing elements within the crustal column. Very high heat-producing rocks must be confined to the uppermost crust so that that crust is thermally and mechanically stable (Sandiford & McLaren, 2002; McLaren *et al.*, 2005). This configuration limits the propagation of high geothermal gradients to shallow crustal levels and lower crustal temperatures remain low. In regions of high average heat production, such as the Mount Painter Province, a 'global-means-approach' is clearly inadequate for understanding the crustal thermal regime and temperature-dependent processes such as metamorphism and magmatism.

The MPP example is remarkable as a consequence of its extreme enrichment in the heat-producing elements. However, the potential generation of crustal melts through the burial of high heat-producing basement rocks may also have implications for the magmatic evolution of other terranes that are characterized by

high concentrations of the heat-producing elements. For example, Gerdes *et al.* (2000) showed that the thickening of high heat-producing units during deformation may account for the timing and generation of widespread granite magmatism in the Variscan Orogen of Europe; Lathrop *et al.* (1994) showed that radiogenic heat production helps to account for mid-crustal anatexis in the Acadian Appalachians. However, in terms of volume, the most notable examples come from other Australian Proterozoic terranes (such as the Mount Isa and Tennant Creek Inliers and the Arunta Province) that are characterized by average surface heat flows around twice global averages for equivalent age terranes elsewhere (McLaren *et al.*, 2003). In many of these terranes voluminous U-, Th- and K-enriched felsic intrusions are known from the Palaeoproterozoic and Mesoproterozoic (McLaren *et al.*, 2005). The geochemical signature of the vast majority (96·2%) of these granites is unlike those of modern subduction or collisional settings and unlike those typical of Archaean terranes (Wyborn *et al.*, 1992; Budd *et al.*, 2001). Typically these granites are I-type and have a geochemical signature of Sr depletion and Y non-depletion that implies derivation from shallow sources in which plagioclase rather than garnet was stable (Singh & Johannes, 1996). On the continent scale the granites also show a consistent signature of negative ε_{Nd} values ranging from –10 to around zero. The less negative values generally characterize the oldest granites and certain rocks of the Arunta and Halls Creek inliers (e.g. Sheppard *et al.*, 2001). The Nd data from the majority of Australian felsic igneous rocks suggest that they were sourced from pre-existing Proterozoic crust with only very limited additional mantle input. The processes responsible for these distinctive granite suites remain an enigmatic problem of Australian geology, as do the origins of the continental-scale heat-producing element enrichment.

The preservation of extremely high heat-producing rocks such as those in the MPP also has implications for the exploitation of geothermal energy resources. Even small volumes of granite with average heat production in the range of the Mount Painter rocks represent an important potential source of geothermal energy, particularly if they occur at relatively shallow depths and are coupled with other favourable conditions, such as overlying sequences of low average thermal conductivity. In addition to the Mount Painter Province, many of the enriched granites in other Australian Proterozoic terranes (McLaren *et al.*, 2003) also represent important potential energy sources. Granites with modern heat production greater than 5 $\mu W/m^3$ crop out over more than 34 000 km^2 and are likely to extend into the near sub-surface. For comparison, the South West England Batholith in Cornwall, one of the best-known geothermal energy resources, has a heat production of between 4 and 5·3 $\mu W/m^3$ (Downing & Gray, 1986). Although recent exploration activity has begun to identify and test possible geothermal energy resources in Australia, much of the potential of these rocks for energy generation remains untapped.

ACKNOWLEDGEMENTS

Fieldwork was undertaken over a period from 1996 to 2001, and the Sprigg family is thanked for their generosity in allowing access to Arkaroola. Richard White generously allowed us to use and publish his NCKFMASH phase equilibria calculations. John Mya and Shane Paxton are thanked for mineral separation, and John Stanley is thanked for technical assistance with the divided-bar apparatus at the University of Adelaide. Our knowledge of the Mount Painter region has benefited from discussions with Eike Paul and John Foden. S.M. and N.N. acknowledge support of Australian Postgraduate awards at the University of Adelaide, and S.M. acknowledges the support of an ARC Australian Postdoctoral Fellowship and Discovery Grant at the ANU. We thank Kurt Stüwe for his detailed and helpful review of the manuscript, and Geoff Clarke for his editorial handling.

SUPPLEMENTARY DATA

Supplementary data for this paper are available at *Journal of Petrology* online.

REFERENCES

Adams, J. A. S., Osmond, K. & Rogers, J. J. W. (1959). The geochemistry of thorium and uranium. *Physics and Chemistry of the Earth* **3**, 298–348.

Barbarin, B. (1996). Genesis of the two main types of peraluminous granitoids. *Geology* **24**, 295–298.

Bell, K., Blenkinsop, J., Cole, T. & Menagh, D. (1982). Evidence from Sr isotopes for long-lived heterogeneities in the upper mantle. *Nature* **298**, 251–253.

Budd, A. R., Wyborn, L. A. I. & Bastrakova, I. V. (2001). The metallogenic potential of Australian Proterozoic granites. *Geoscience Australia Record* **2001/12**.

Chappell, B. W. (1996). Compositional variation within granite suites of the Lachlan Fold Belt; its causes and implications for the physical state of granite magma. *Geological Society of America, Special Papers* **315**, 159–170.

Chappell, B. W. & White, A. J. R. (1974). Two contrasting granite types. *Pacific Geology* **8**, 173–174.

Christensen, N. I. & Mooney, W. D. (1995). Seismic velocity structure and composition of the continental crust; a global view. *Journal of Geophysical Research* **100**, 9761–9788.

Compston, W., Williams, I. S., Meyer, C. E., Boynton, W. V. E. & Schubert, G. E. (1984). U–Pb geochronology of zircons from lunar breccia 73217 using a sensitive high mass-resolution ion microprobe. *Journal of Geophysical Research* **89**, 525–534.

Cull, J. P. (1982). An appraisal of Australian heat-flow data. *Bureau of Mineral Resources Journal of Australian Geology and Geophysics* **7**, 11–21.

Dickin, A. P. (1997). *Radiogenic Isotope Geology*. Cambridge: Cambridge University Press.

Dovenyi, P. & Horvath, F. (1988). A review of temperature, thermal conductivity and heat flow data for the Pannonian Basin. In: Royden, L. H. & Horvath, F. (eds) *The Pannonian Basin: a Study in Basin Evolution. American Association of Petroleum Geologists, Memoirs* **45**, 195–233.

Downing, R. A. & Gray, D. A. (1986). Geothermal resources of the United Kingdom. *Journal of the Geological Society, London* **143**, 499–507.

Durrance, E. M. (1986). *Radioactivity in Geology: Principles and Applications*. New York: Halstead Press.

Elburg, M. A., Bons, P. D., Dougherty-Page, J., Janka, C. E., Neumann, N. & Schaefer, B. (2001). Age and metasomatic alteration of the Mt Neil Granite, Nooldoonooldoona Waterhole, Mt Painter Inlier, South Australia. *Australian Journal of Earth Sciences* **48**, 721–730.

Elburg, M. A., Bons, P. D., Foden, J. & Brugger, J. (2003). A newly defined Late Ordovician magmatic–thermal event in the Mount Painter Province, northern Flinders Ranges, South Australia. *Australian Journal of Earth Sciences* **50**, 611–631.

Fanning, C. M. (1995). Geochronological synthesis of southern Australia. Part 1. The Curnamona Province. Adelaide, South Australia: Department of Mines and Energy, Open file envelope. (unpublished).

Foden, J., Sandiford, M., Dougherty-Page, J. & Williams, I. (1999). Geochemistry and geochronology of the Rathjen gneiss; implications for the early tectonic evolution of the Delamerian Orogen. *Australian Journal of Earth Sciences* **46**, 377–389.

Foden, J., Song, S. H., Turner, S. P., Elburg, M. A., Smith, P. B., Van Der Steldt, B. & Van Penglis, D. (2002). Geochemical evolution of lithospheric mantle beneath S.E. South Australia. *Chemical Geology* **182**, 663–695.

Frei, R. & Kamber, B. S. (1995). Single mineral Pb–Pb dating. *Earth and Planetary Science Letters* **129**, 261–286.

Gerdes, A., Worner, G. & Henk, A. (2000). Post-collisional granite generation and HT–LP metamorphism by radiogenic heating: the Variscan South Bohemian Batholith. *Journal of the Geological Society, London* **157**, 577–587.

Goldstein, S. L., O'Nions, R. K. & Hamilton, P. J. (1984). A Sm–Nd study of atmospheric dusts and particulates from major river systems. *Earth and Planetary Science Letters* **70**, 221–236.

Haenel, R., Rybach, L. & Stegena, L. (eds) (1998). *Handbook of Terrestrial Heat-flow Density Determination; with Guidelines and Recommendations of the International Heat Flow Commission*. Dordrecht: Kluwer Academic.

Holland, T. J. B. & Powell, R. (1998). An internally-consistent thermodynamic dataset for phases of petrological interest. *Journal of Metamorphic Geology* **16**, 309–344.

Holland, T. J. B. & Powell, R. (2001). Calculation of phase relations involving haplogranitic melts using an internally-consistent thermodynamic dataset. *Journal of Petrology* **42**, 673–683.

Houseman, G. A., Cull, J. P., Muir, P. M. & Peterson, H. L. (1989). Geothermal signatures and uranium ore deposits on the Stuart Shelf of South Australia. *Geophysics* **54**, 158–170.

Jaupart, C. & Mareschal, J. C. (1999). The thermal structure and thickness of continental roots. *Lithos* **48**, 93–114.

Jenkins, R. J. F. & Sandiford, M. (1992). Observations on the tectonic evolution of the southern Adelaide Fold Belt. *Tectonophysics* **214**, 27–36.

Johnson, G. I. (1980). The geology of the Mount Babbage Inlier, northern Mount Painter Province, South Austrlaia—a petrological, geochemical and geochronological study. B.Sc.(Hons) thesis, University of Adelaide.

Lathrop, A. S., Blum, J. D. & Chamberlain, C. P. (1994). Isotopic evidence for closed-system anatexis at midcrustal levels: an example from the Acadian Appalachians of New England. *Journal of Geophysical Research* **99**, 9453–9468.

Mawby, J., Hand, M. & Foden, J. (1999). Sm–Nd evidence for high-grade Ordovician metamorphism in the Arunta Block, central Australia. *Journal of Metamorphic Geology* **17**, 653–668.

McLaren, S., Sandiford, M. & Hand, M. (1999). High-heat producing granites and metamorphism—an example from the Mount Isa Inlier, Australia. *Geology* **27**, 679–682.

McLaren, S., Dunlap, W. J., Sandiford, M. & McDougall, I. (2002). Thermochronology of high heat producing crust at Mount Painter, South Australia: implications for tectonic reactivation of continental interiors. *Tectonics* **21**(4), doi:10.1029/2000TC001275.

McLaren, S., Sandiford, M., Hand, M., Neumann, N., Wyborn, L. & Bastrakova, I. (2003). The hot southern continent: heat flow and heat production in Australian Proterozoic terranes. In: Hillis, R. & Muller, D. (eds). *Geological Society of Australia* **22**, *The Evolution and Dynamics of the Australian Plate*, 151–161.

McLaren, S., Sandiford, M. & Powell, R. (2005). Contrasting styles of Proterozoic crustal evolution: a hot-plate tectonic model for Australian terranes. *Geology* **33**, 673–676.

McLennan, S. M. & Taylor, S. R. (1996). Heat flow and the chemical composition of continental crust. *Journal of Geology* **104**, 369–377.

Mildren, S. & Sandiford, M. (1995). A heat refraction mechanism for low-*P* metamorphism in the northern Flinders Ranges, South Australia. *Australian Journal of Earth Sciences* **42**, 241–247.

Miller, C. F. & Bradfish, L. J. (1980). An inner Cordilleran belt of muscovite-bearing plutons. *Geology* **8**, 412–416.

Neumann, N. L. (2001). Geochemical and isotopic characteristics of South Australian Proterozoic granites: implications for the origin and evolution of high heat-producing terrains. Ph.D. thesis, University of Adelaide.

Neumann, N., Sandiford, M. & Foden, J. (2000). Regional geochemistry and continental heat flow: implications for the origin of the South Australian heat flow anomaly. *Earth and Planetary Science Letters* **183**, 107–120.

Nyblade, A. A. & Pollack, H. N. (1993). A global analysis of heat flow from Precambrian terrains: implications for the thermal structure of Archaean and Proterozoic lithosphere. *Journal of Geophysical Research* **98**, 12207–12218.

O'Halloran, G. (1992). The evolution of provenance and depositional processes during early Adelaidean sedimentation. A sedimentational and Nd isotopic investigation. B.Sc.(Hons) thesis, University of Adelaide.

Paul, E. G., Flottmann, T. & Sandiford, M. (1999). Structural geometry and controls on basement-involved deformation in the northern Flinders Ranges, Adelaide fold belt, South Australia. *Australian Journal of Earth Sciences* **46**, 343–354.

Periera, E. B., Hamza, V. M., Furtado, V. & Adams, J. A. S. (1986). U, Th and K content, heat production and thermal conductivity of São Paulo, Brazil, continental shelf sediments: a reconnaissance work. *Chemical Geology* **58**, 217–226.

Powell, R., Holland, T. J. B. & Worley, B. (1998). Calculating phase diagrams involving solid solutions via non-linear equations, with examples using THERMOCALC. *Journal of Metamorphic Geology* **16**, 577–588.

Powell, R., Woodhead, J. & Hergt, J. (2002). Improving isochron calculations with robust statistics and the bootstrap. *Chemical Geology* **185**, 191–204.

Preiss, W. V. (2000). The Adelaide Geosyncline of South Australia and its significance in Neoproterozoic continental reconstruction. *Precambrian Research* **100**, 21–63.

Rudnick, R. L. & Fountain, D. (1995). Nature and composition of the continental crust: a lower crustal perspective. *Reviews of Geophysics* **33**, 267–309.

Rudnick, R. L., McDonough, S. M. & O'Connell, R. J. (1998). Thermal structure, thickness and composition of continental lithosphere. *Chemical Geology* **145**, 395–411.

Sandiford, M. (2003). Neotectonics of southeastern Australia: linking the Quaternary faulting record with seismicity and *in situ* stress. In: Hillis, R. & Muller, D. (eds). *Geological Society of Australia, Special Publications* **22**, *The Evolution and Dynamics of the Australian Plate*, 101–113.

Sandiford, M. & Hand, M. (1998). Controls on the locus of Phanerozoic intraplate deformation in central Australia. *Earth and Planetary Science Letters* **162**, 97–110.

Sandiford, M. & McLaren, S. (2002). Tectonic feedback and the ordering of heat producing elements within the continental lithosphere. *Earth and Planetary Science Letters* **204**, 133–150.

Sandiford, M. & McLaren, S. (2006). Thermo-mechanical controls on heat production distributions and the long-term evolution of the continents. In: Brown, M. & Rushmer, T. (eds) *Evolution and Differentiation of the Continental Crust*. Cambridge: Cambridge University Press, pp. 67–91.

Sandiford, M., Hand, M. & McLaren, S. (1998). High geothermal gradient metamorphism during thermal subsidence. *Earth and Planetary Science Letters* **163**, 149–165.

Sandiford, M., McLaren, S. & Neumann, N. (2002). Long-term thermal consequences of the redistribution of heat-producing elements associated with large-scale granitic complexes. *Journal of Metamorphic Geology* **20**, 87–98.

Sass, J. H. & Lachenbruch, A. H. (1979). Thermal regime of the Australian continental crust. In: McElhinny, M. W. (ed.) *The Earth—its Origin, Structure and Evolution*. London: Academic Press, pp. 301–351.

Sass, J. H., Jaeger, J. C. & Munroe, R. J. (1976). Heat flow and near surface radioactivity in the Australian continental crust. *US Geological Survey, Open-File Report* **76-250**.

Schaefer, B. F. (1993). Isotopic and geochemical constraints on Proterozoic crustal growth of the Mount Painter Inlier. B.Sc.(Hons) thesis, University of Adelaide.

Scrimgeour, I. & Raith, J. G. (2001). High-grade reworking of Proterozoic granulites during Ordovician intraplate transpression, eastern Arunta Inlier, central Australia. In: Miller, J. A., Buick, I. S., Hand, M. & Holdsworth, R. E. (eds) *Continental Reworking and Reactivation. Geological Society, London, Special Publications* **184**, 261–287.

Shaw, D. M., Cramer, J. J., Higgins, M. D. & Truscott, M. G. (1986). Composition of the Canadian Precambrian Shield and the continental crust of the Earth. In: Dawson, J. B., Carswell, D. A., Hall, J. & Wedepohl, K. H. (eds) *The Nature of the Lower Continental Crust. Geological Society, London, Special Publications* **24**, 275–282.

Sheard, M. J., Fanning, C. M. & Flint, R. B. (1992). Geochronology and definition of Mesoproterozoic volcanics and granitoids of the Mount Babbage Inlier, northern Flinders Ranges. *Geological Survey of South Australia Quarterly Geological Notes* **123**, 18–32.

Sheppard, S., Griffin, T. J., Tyler, I. M. & Page, R. W. (2001). High- and low-K granites and adakites at a Palaeoproterozoic plate boundary in northwestern Australia. *Journal of the Geological Society, London* **158**, 547–560.

Simons, F. J., Zuber, M. T. & Korenaga, J. (2000). Isostatic response of the Australian lithosphere; estimation of effective elastic thickness and anisotropy using multitaper spectral analysis. *Journal of Geophysical Research* **105**, 19163–19184.

Singh, J. & Johannes, W. (1996). Dehydration melting of tonalities: Part II, Composition of melts and solids. *Contributions to Mineralogy and Petrology* **125**, 26–44.

Stacey, J. S. & Kramers, J. D. (1975). Approximation of terrestrial lead isotope evolution by a two-stage model. *Earth and Planetary Science Letters* **26**, 207–221.

Sun, S. S. & McDonough, W. F. (1989). Chemical and isotopic systematics of oceanic basalts; implications for mantle composition and processes. In: Saunders, A. D. & Norry, M. J. (eds) *Magmatism in the Ocean Basins. Geological Society, London, Special Publications* **42**, 313–345.

Taylor, S. R. & McLennan, S. M. (1981). The composition and evolution of the continental crust: rare earth element evidence from sedimentary rocks. *Philosophical Transactions of the Royal Society of London, Series A* **301**, 381–399.

Taylor, S. R. & McLennan, S. M. (1985). *The Continental Crust: its Composition and Evolution*. Oxford: Blackwell Scientific.

Teale, G. S. (1979). Revision of nomenclature for Palaeozoic intrusives of the Mount Painter Province, South Australia. *Transactions of the Royal Society of South Australia* **103**, 119–131.

Teale, G. S. (1993). The Mount Painter and Mount Babbage Inliers. In: Drexel, J. F., Preiss, W. V. & Parker, A. J. (eds) *The Geology of South Australia, Volume 1, The Precambrian. South Australian Geological Survey Bulletin,* **54**, 93–100.

Thornton, G. D. (1980). Geology, geochemistry and geochronology of the eastern Babbage Block, Mount Painter Province, South Australia. B.Sc.(Hons) thesis, University of Adelaide.

Vigneresse, J. L., Barbey, P. & Cuney, M. (1996). Rheological transitions during partial melting and crystallization with application to felsic magma segregation and transfer. *Journal of Petrology* **37**, 1579–1600.

Weaver, B. J. & Tarney, J. (1984). Major and trace element composition of the continental lithosphere. *Physics and Chemistry of the Earth* **15**, 39–68.

Wedepohl, K. H. (1995). The composition of the continental crust. *Geochimica et Cosmochimica Acta* **59**, 1217–1232.

White, R. W., Powell, R. & Holland, T. J. B. (2001). Calculation of partial melting equilibria in the system CaO–Na_2O–K_2O–FeO–MgO–Al_2O_3–SiO_2–H_2O (CNKFMASH). *Journal of Metamorphic Geology* **19**, 139–153.

White, R. W., Pomroy, N. E. & Powell, R. (2005). An *in situ* metatexite–diatexite transition in upper amphibolite facies rocks from Broken Hill, Australia. *Journal of Metamorphic Geology* **23**, 579–602.

Williams, I. S. (1998). U–Th–Pb geochronology by ion microprobe. In: McKibben, M. A., Shanks, W. C. P.,III & Ridley, W. I. (eds) *Applications of Microanalytical Techniques to Understanding Mineralizing Processes. Society of Economic Geologists, Short Courses* **7**, 1–35.

Wyborn, L. A. I., Wyborn, D., Warren, R. G. & Drummond, B. J. (1992). Proterozoic granite types in Australia: implications for lower crust composition, structure and evolution. *Transactions of the Royal Society of Edinburgh: Earth Sciences* **83**, 201–209.